Journal of Statistical Physics, Vol. 35, Nos. 5/6, 1984

Local and Global Behavior near Homoclinic Orbits

Paul Glendinning[1] and Colin Sparrow[2]

Received November 8, 1983

We study the local behavior of systems near homoclinic orbits to stationary points of saddle-focus type. We explicitly describe how a periodic orbit approaches homoclinicity and, with the help of numerical examples, discuss how these results relate to global patterns of bifurcations.

KEY WORDS: Bifurcations; chaos; homoclinic orbits; period-doubling.

1. INTRODUCTION

Some ordinary differential equations are known to have homoclinic orbits to stationary points of a saddle-focus type. These orbits tend towards the stationary point in both forwards and backwards time, approaching the point directly in one time direction (along a vector associated with a real eigenvalue of the flow linearized near the stationary point) and spiraling into the point in the other time direction (on a plane associated with a complex conjugate pair of eigenvalues of the linearized flow).

There is a confusion in the literature between the local and global effects of such a homoclinic orbit in a system of equations. Sil'nikov[1,2] proved some theorems about the existence of periodic and aperiodic trajectories in a neighborhood of these homoclinic orbits, some of which have been improved or added to in recent years. At the same time, other writers have attempted to relate these local results to numerically observed chaotic behaviors in systems of equations in which the appropriate types of

[1] Department of Applied Mathematics and Theoretical Physics, Silver Street, Cambridge, U.K.

[2] Department of Pure Mathematics and Mathematical Statistics, Mill Lane, Cambridge, U.K.

0022-4715/84/0600-0645$03.50/0

homoclinic orbit occur. There is, undoubtedly, some relationship between these two phenomena, but we believe that it has often been stated oversimply. In this paper we explore the relationship between the local (theoretical) results and the global (observed) behaviors in more detail; our arguments will be a combination of theoretical, numerical, and intuitive ideas, and throughout the paper we have emphasized understanding over rigor.

We start, in Section 2, by repeating a by now standard analysis of the local behavior near to a homoclinic orbit. This gives us a two-dimensional return map on a section of a plane close to the relevant stationary point, and it is this map which we analyze in Section 3. Our main aim is not to reprove Sil'nikov's theorems; instead we concentrate on the fixed points of the map and obtain explicit results about how a periodic orbit approaches homoclinicity as a parameter is varied around the value at which we have homoclinicity. In some situations this approach is through an infinite number of tangent (saddle-node) bifurcations. We can calculate quantities which relate the period of the orbit and parameter values as the orbit approaches homoclinicity to the eigenvalues at the stationary point. We also show that there may be an infinite sequence of homoclinic orbits close to the one which we are considering. Throughout Section 3 we emphasize those results which will be useful when trying to piece together global bifurcation pictures for systems which have the appropriate type of homoclinic orbit. In particular, we argue that it may sometimes be legitimate and useful to think (in global terms) of the many bifurcations that may occur close to homoclinicity as producing, collectively, a single periodic orbit.

In Section 4 we study three different systems of ordinary differential equations. In Section 4.1 we examine the Lorenz equations; these illustrate the theoretical results in a very convincing fashion (and in the presence of a symmetry). In Section 4.2 we study a very different system, and our emphasis here is on producing a fairly complete bifurcation picture for a wide range of parameters. This involves, amongst other things, drawing a distinction between those aspects of the observed behavior which can be properly predicted from the local analysis near each homoclinic orbit, and those aspects of the behavior which should more properly be inferred from global properties of the flow deriving from an interaction between two stationary points. This distinction is emphasized by Section 4.3, where we study a system similar to that of Section 4.2 but which is piecewise linear; for the system of Section 4.3 we show how the development of numerically observed chaotic behavior can be comprehended with only the crudest understanding of homoclinic orbits.

Finally, in Section 5, we indicate the likely implications of our work for other systems of equations containing homoclinic orbits of the appropriate kind, and mention some of these.

2. A TWO-DIMENSIONAL RETURN MAP ON A SURFACE NEAR THE STATIONARY POINT

We consider one-parameter families of autonomous ordinary differential equations which can be written in the form

$$\dot{x} = -\lambda_2 x - \omega y + P(x, y, z; \mu)$$

$$\dot{y} = \omega x - \lambda_2 y + Q(x, y, z; \mu)$$

$$\dot{z} = \lambda_1 z + R(x, y, z; \mu)$$

with $\lambda_1, \lambda_2 > 0$ and P, Q, R analytic functions of x, y, z and μ which vanish with their first derivatives when $x = y = z = 0$. The origin ($x = y = z = 0$) is thus a stationary point of saddle type with linearized eigenvalues λ_1, $-\lambda_2 \pm i\omega$. Suppose that when $\mu = 0$ the unstable manifold of the origin is included in the stable manifold of the origin, so there is a homoclinic orbit (an orbit which tends to the origin as $t \to \pm\infty$). Without loss of generality we can choose our parameter μ so that the flow looks like that illustrated in Fig. 2.1 for parameter values $\mu < 0$, $\mu = 0$, and $\mu > 0$. We wish to calculate a two-dimensional return map (Poincaré map) on some suitable surface close to the stationary point for μ values near zero. Our derivation follows Arneodo *et al.*[3] almost exactly, though we consider a slightly more general case. See also Refs. 4–7.

The map is obtained by dividing the flow close to the stationary point and its unstable manifold into two parts: a small neighborhood of the stationary point where the flow is essentially linear, and a global flow which takes trajectories close to the unstable manifold away from and then back into the linear region. The reader interested in a detailed justification of this procedure should consult Refs. 7, 3, 8, or 9.

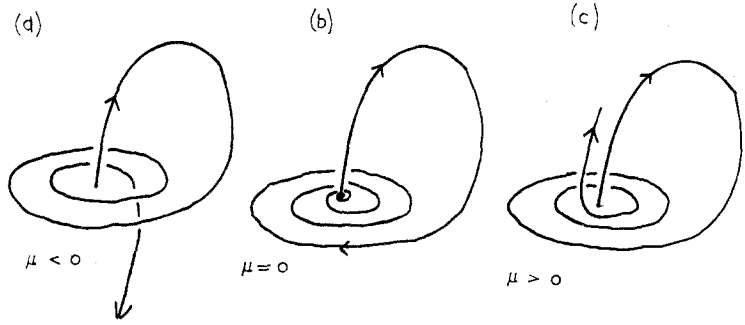

Fig. 2.1. Behavior of the unstable manifold of the origin. (a) $\mu < 0$; (b) $\mu = 0$; (c) $\mu > 0$.

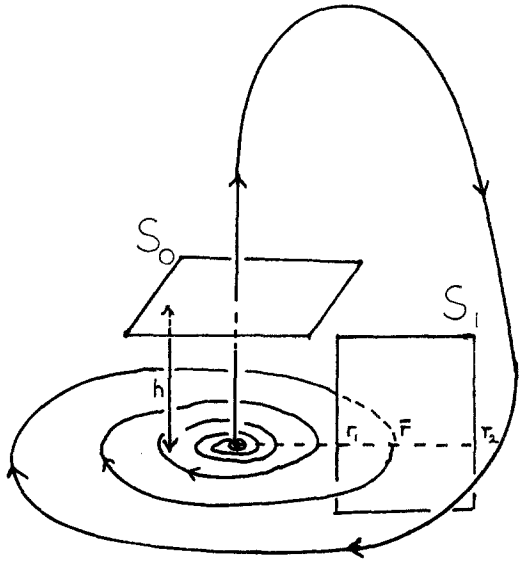

Fig. 2.2. The surfaces used to calculate the return map, illustrated at $\mu = 0$. S_0 is parallel to the stable manifold and a distance h above it. S_1 is perpendicular to this manifold. The unstable manifold strikes S_1 a distance $\bar{r}$ from the stationary point; we consider only a strip of S_1 such that each trajectory only strikes S_1 once as it spirals into the stationary point $[r_1 = r_2 \exp(-2\pi\lambda_2/\omega)]$.

The situation is illustrated in Fig. 2.2. Inside the linear region containing the stationary point we choose two surfaces: S_0 is parallel to the stable manifold of the stationary point and a distance h above it; S_1 is perpendicular to the stable manifold, intersecting it on a radial line out from the stationary point. We shall derive the return map $\Sigma_\mu : S_1 \to S_1$ by using the linearization assumption to obtain a map $\Sigma^1 : S_1 \to S_0$ and then find a map $\Sigma^0_\mu : S_0 \to S_1$ which specifies how trajectories which leave S_0 into the nonlinear region return to the linear region at S_1.

We use cylindrical polar coordinates (r, θ, z) with the stationary point at the origin and the stable manifold of the origin (in the linear region) on the plane $(r, \theta, 0)$. In these coordinates S_0 is a part of the plane (r, θ, h) and S_1 a part of the plane $(r, 0, z)$. In the linear region the differential equations are given by

$$\begin{aligned} \dot{r} &= -\lambda_2 r \\ \dot{\theta} &= \omega \\ \dot{z} &= \lambda_1 z \end{aligned} \tag{1}$$

which have solutions

$$\begin{aligned} r(t) &= r_0 e^{-\lambda_2 t} \\ \theta(t) &= \theta_0 + \omega t \\ z(t) &= z_0 e^{\lambda_1 t} \end{aligned} \tag{2}$$

Thus, a trajectory started at $(r_0, 0, z_0)$ on ω_1 strikes S_0 at time T where $h = z_0 e^{\lambda_1 T}$ providing $z_0 > 0$. If $z_0 < 0$, the trajectory wanders away from the region we are considering and is of no further interest in this local analysis (see Fig. 2.1). This gives us, for $z_0 > 0$, a map $\Sigma^1 : S_1 \to S_0$ given by

$$\Sigma^1(r_0, 0, z_0) \to \left(r_0 \left(\frac{z_0}{h} \right)^{\lambda_2/\lambda_1}, \frac{\omega}{\lambda_1} \ln\left(\frac{h}{z} \right), h \right) \tag{3}$$

We now consider the map $\Sigma_\mu^0 : S_0 \to S_1$. We have assumed that when $\mu = 0$ there is a homoclinic orbit. Thus we have $\Sigma_0^0(0, 0, h) = (\bar{r}, 0, 0)$ and, from our choice of parameter in Fig. 2.1, we have $\Sigma_\mu^0(0, 0, h) = (r, 0, z)$, with z having the same sign as μ; these equations give us the behavior of the unstable manifold of the origin. If the region we are considering is small enough we may assume that the remainder of Σ_μ^0 is given by first-order linear terms in a Taylor expansion. This gives us $\Sigma_\mu^0 : S_0 \to S_1$ given by

$$\begin{aligned} \Sigma_\mu^0(r, \theta, h) = (&\bar{r} + a\mu + br\cos\theta + cr\sin\theta, 0, \\ &d\mu + er\cos\theta + fr\sin\theta) \end{aligned} \tag{4}$$

with a, b, c, d, e, and f constants depending on the global flow (such that the map is nonsingular) with $d > 0$.

Equation (4) can be rewritten

$$\Sigma_\mu^0(r, \theta, h) = \left(\bar{r} + a\mu + pr\cos(\theta + \phi_1), 0, d\mu + qr\cos(\theta + \phi_2) \right) \tag{5}$$

Combining Eqs. (3) and (5) we obtain a map $\Sigma_\mu : S_1 \to S_1$ (dropping the middle coordinate, which is zero) given by

$$\begin{aligned} \Sigma_\mu(r, z) = \Bigg(&\bar{r} + a\mu + pr\left(\frac{z}{h} \right)^{\lambda_2/\lambda_1} \cos\left[\frac{\omega}{\lambda_1} \ln\left(\frac{h}{z} \right) + \phi_1 \right], \\ &d\mu + qr\left(\frac{z}{h} \right)^{\lambda_2/\lambda_1} \cos\left[\frac{\omega}{\lambda_1} \ln\left(\frac{h}{z} \right) + \phi_2 \right] \Bigg) \end{aligned} \tag{6}$$

We may simplify this equation by writing constants

$$\delta = \lambda_2/\lambda_1, \qquad \alpha = ph^{-\delta}, \qquad \beta = qh^{-\delta}$$

$$\xi = -\frac{\omega}{\lambda_1}, \qquad \Phi_1 = \frac{\omega}{\lambda_1} \ln h + \phi_1, \qquad \Phi_2 = \frac{\omega}{\lambda_1} \ln h + \phi_2$$

and by rescaling the parameter μ so that $d = 1$. We then have

$$\Sigma_\mu(r, z) = \big(\bar{r} + a\mu + \alpha r z^\delta \cos(\xi \ln z + \Phi_1),$$
$$\mu + \beta r z^\delta \cos(\xi \ln z + \Phi_2)\big) \tag{7}$$

Recall that Eq. (7) is defined only for $z > 0$ and for r in a certain range chosen so that trajectories only pierce S_1 once as they spiral towards the origin (see caption to Fig. 2.2), and that δ, the constant which determines the relative sizes of the eigenvalues at the stationary point ($\delta = \lambda_2/\lambda_1$), is positive.

Notes on the Validity of Equation (7)

(1) We should only use results obtained from the return map (7) when we can be reasonably certain that the properties of this map accurately reflect the topological and stability properties of the actual flow under consideration. As explained above, the procedure we used to derive (7) can be formally justified, but only in some unspecified neighborhood of the homoclinic orbit. Consequently, we should only rely on (7) when r, z, and μ are all small.

(2) We have assumed that the eigenvalues λ_1, $-\lambda_2 \pm i\omega$, are constant with changing μ. This is actually an unnecessarily restrictive assumption, made to simplify the formulas. We are free to use (7) even if this assumption does not hold, unless δ ($= \lambda_2/\lambda_1$) is at a critical value (we shall see in Section 3 that $\delta = 1$ is critical).

(3) We have assumed that we are not interested in trajectories that start on S_1 with $z < 0$. These trajectories will move away from the station-

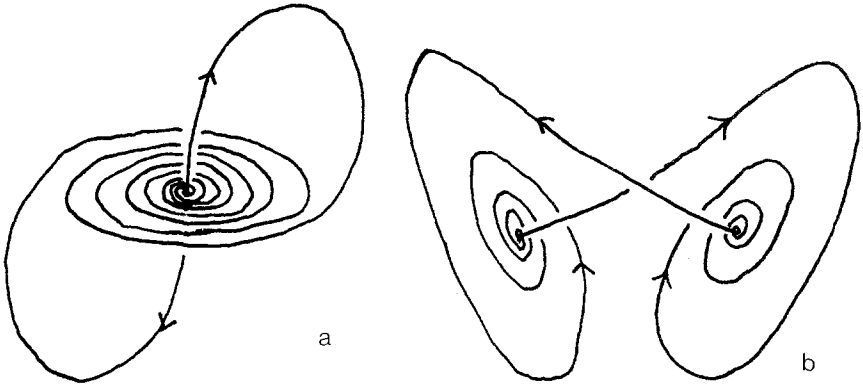

Fig. 2.3. Two types of symmetric situation in which the return map (7) will be useful.

ary point near to the branch of the unstable manifold which we have not considered. In many systems this is sensible as, for example, this branch of the manifold often tends to infinity without coming close to the stationary point again. It is clear, however, that in certain circumstances, for instance if there is a symmetry like that shown in Fig. 2.3a, our derivation will apply for $z < 0$ as well as for $z > 0$ (with the obvious changes in sign). We do not consider the case shown in Fig. 2.3a any further. Note, though, that Eq. (7) will be almost directly applicable to the type of symmetric situation shown in Fig. 2.3b. We consider this case again when we look at the Lorenz equations in Section 4.

3. ANALYSIS OF THE MAP

We analyze Eq. (7) of Section 2 in its full two-dimensional form. We concentrate mainly on the simplest fixed points of (7), partly because a more general analysis is complicated, but mainly because this study will give results likely to be of direct interest when we perform numerical experiments on examples. In fact, as we shall see, our analysis gives a surprising wealth of information. Some of the results below are immediate corollaries of Sil'nikov's theorems. We shall state these theorems in due course.

3.1. Fixed Points of the Map

3.1.1. Number of Fixed Points ($z, \mu \ll 1$). If we put the left and right sides of Eq. (7) equal we obtain, for the r coordinate,

$$r = (\bar{r} + a\mu)/\left[1 - \alpha z^{\delta}\cos(\xi \ln z + \Phi_1)\right] \tag{8}$$

Substituting (8) into the equation for the z coordinate we get

$$(z - \mu)\left[1 - \alpha z^{\delta}\cos(\xi \ln z + \Phi,)\right] = (\bar{r} + a\mu)\,\beta z^{\delta}\cos(\xi \ln z + \Phi_2) \tag{9}$$

Calculating the position and number of intersections of the two curves representing the left and right sides of (9) is, in general, complicated, but if we restrict our attention to the region $z \ll 1$ so that the left side of (9) becomes approximately $z - \mu$, our task is considerably simplified. Each diagram in Fig. 3.1 shows, for a particular choice of parameters δ and μ, two curves representing the left and right sides of Eq. (9), respectively. The points of intersection of the two curves give the z values of fixed points of (7). (Notice particularly that these diagrams are *not* one-dimensional maps.)

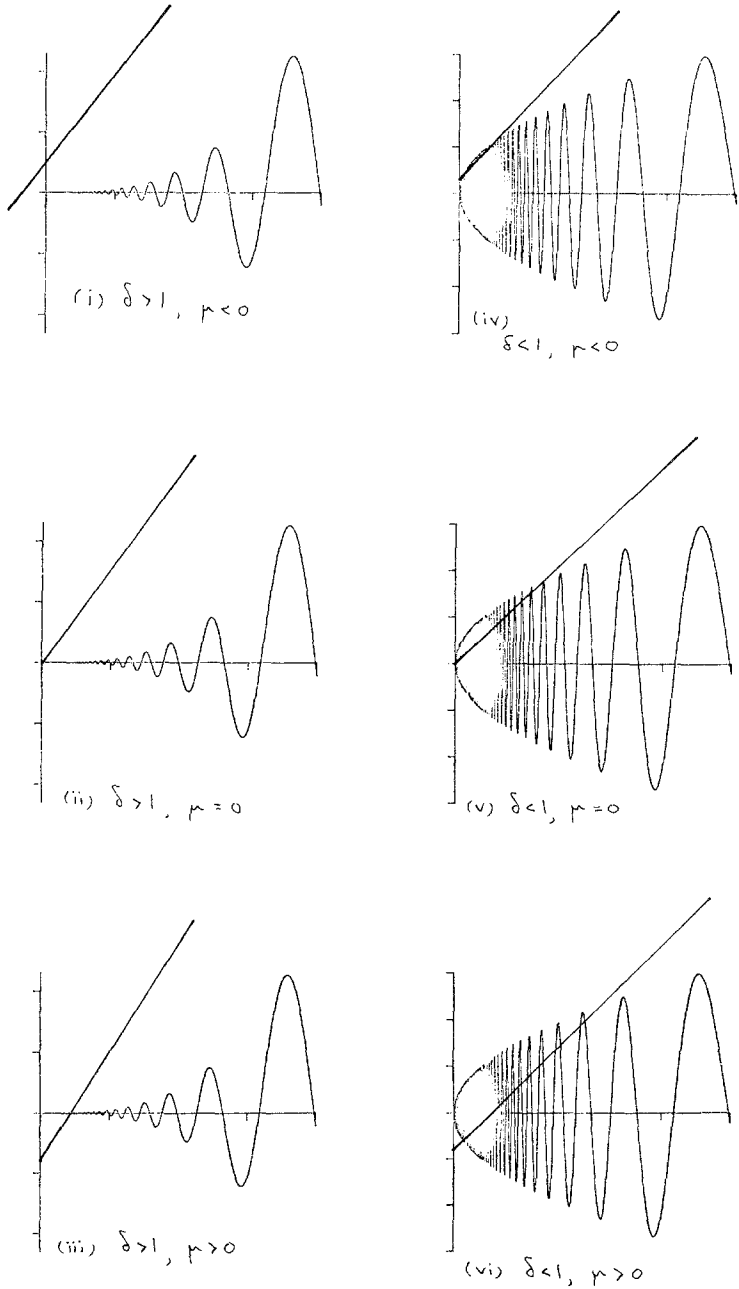

Fig. 3.1. The curves $z - \mu$ and $\beta z^{\delta}\cos(\xi \ln z + \Phi_2)$ for various values of μ and δ. Intersections of the curves give the z coordinate of fixed points of the return map (7). (i)–(iii) $\delta > 1$; (iv)–(vi) $\delta < 1$.

For $\delta > 1$ [diagrams (i)–(iii) of Fig. 3.1] we have the following:

(i) and (ii) $\mu \leqslant 0$. There are no fixed points of (7) in $z \ll 1$ except for the one at $z = \mu = 0$. This fixed point lies on the homoclinic orbit which exists at $\mu = 0$.

(iii) $\mu > 0$. In $z \ll 1$ there is one fixed point of (7) for each μ. [The slope of the wiggly curve in Fig. 3.1(iii) has order $z^{\delta - 1}$ which is small since $\delta > 1$. This implies the existence of only one intersection of the two curves.] This fixed point will lie on a periodic orbit of the original differential equations which passes once through the region of the linear analysis near the stationary point before closing up.

When $\delta < 1$ [diagrams (iv)–(vi) of Fig. 3.1] we have the following:

(iv) and (vi) $\mu < 0$ and $\mu > 0$. There is a finite number of intersections of the two curves, each representing a fixed point of (7) lying on some periodic orbit of the original differential equations which passes once through the region of the linear analysis near the stationary point.

(v) $\mu = 0$. There is a countable infinity of intersections representing a countable infinity of periodic orbits in the original equations.

3.1.2. Bifurcation Diagrams. Period of the Orbits. We may summarize the information from 3.1.1 in the two diagrams of Fig. 3.2. Each diagram plots the period of the orbit represented by the fixed points found

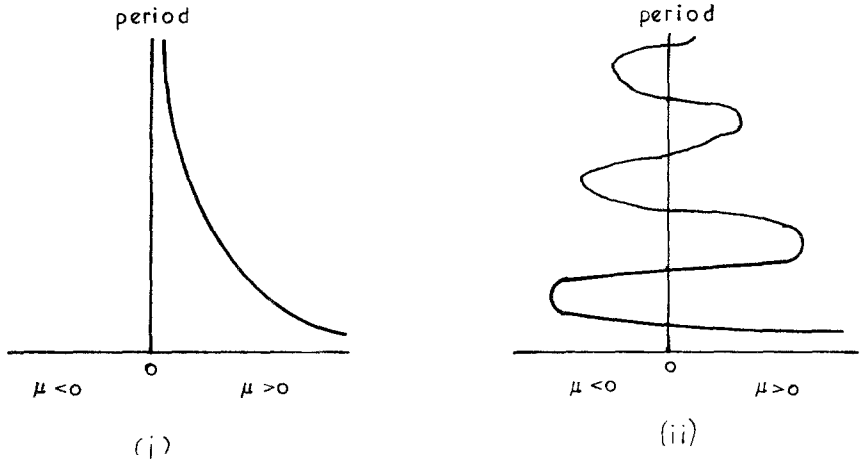

Fig. 3.2. The period of the orbit on which the fixed points of the return map (7) lie. Period is plotted against parameter, μ. (i) $\delta > 1$; (ii) $\delta < 1$.

above against the parameter μ at which they occur. Figure 3.2(i) shows the situation for $\delta > 1$ and Fig. 3.2(ii) shows the situation for $\delta < 1$.

In constructing Fig. 3.2 we have used the fact that the periodic orbits represented by fixed points of (7) with smaller z coordinate twist around the unstable manifold of the stationary point more often [see the derivation of (7) in Section 2]; hence, on the assumption that the time of return to the region of the linear analysis (the time taken to get from S_0 to S_1 in Section 2) is approximately constant, these orbits have longer period. Figure 3.2(i) is fairly straightforward; as μ decreases to zero ($\delta > 1$), the fixed point has z coordinate decreasing to zero, and the period of the orbit through the fixed point increases to infinity. We may say, if we like, that the homoclinic orbit occurring at $\mu = 0$ is a periodic orbit of period infinity. Figure 3.2(ii) is more complicated, but if we consider any fixed μ (a vertical line on Fig. 3.2) we find the number of orbits existing at that μ value agrees with the results of Section 3.1.1 above; if $\mu \neq 0$ a vertical line on Fig. 3.2(ii) intersects the curve in a finite number of points, and if $\mu = 0$ we see an infinite number of intersections.

Figure 3.2(ii) illustrates that there is a sense in which we can say that all of the fixed points of (7) ($\delta < 1$) represent the same periodic orbit; by following the orbit with increasing and decreasing μ we can get continuously from any point of the curve in Figure 3.2(ii) to any other. We may say, in fact, that all the fixed points of (7), for both $\delta > 1$ and $\delta < 1$, lie on one periodic orbit, which we shall call the *principal periodic orbit*, whose period tends to infinity as μ tends to zero. Intuitively speaking, the orbit tends to infinite period by "winding itself up around the unstable manifold of the stationary point" as μ approaches zero. With this interpretation of the results, the difference between the two cases then lies in the way in which we must make μ tend to zero in order to follow the orbit to homoclinicity. When we come to look at examples, the importance of this difference will depend on the size of the wiggles in Fig. 3.2(ii) compared with the size of the parameter range in which we are interested; in other words, we may not be very interested in the difference if we are considering a global and not a local picture (cf. Section 3.3.2).

We can get some idea of the rate at which the wiggles decrease in size, as well as other asymptotic properties of the curves shown in Fig. 3.2 from the information contained in Fig. 3.1. First notice that if we have two fixed points of (7) (at the same or different μ values) such that the z coordinates of these points are z_i and z_{i+1} with $|\xi \ln z_i - \xi \ln z_{i+1}| = \gamma\pi$, the periodic orbits on which these points lie will have periods p_i and p_{i+1} with $|p_i - p_{i+1}| \approx \gamma\pi/\omega$; this follows because $\xi \ln z$ is the quantity which controls the number of rotations about the unstable manifold of the stationary point within the region of linear analysis, and ω is the rate of rotation. With $\delta > 1$

we see that the fixed point satisfies, asymptotically, $z \approx \mu$, and hence can deduce at once that as μ tends to zero from above, the period of the single orbit which exists in $\mu > 1$ tends to infinity like $|\xi(\ln \mu)/\omega|$. Remembering that $\xi = -\omega/\lambda_1$, we have, for Fig. 3.2(i)

$$\text{period} \sim -(\ln \mu)/\lambda_1 \tag{10}$$

For $\delta < 1$ we consider the period of the orbit at the various intersections of the bifurcation curve with $\mu = 0$. If we write these as p_i, p_{i+1}, p_{i+2}, etc., we have

$$\lim_{i \to \infty} (p_{i+1} - p_i) = \pi/\omega \tag{11}$$

since fixed points occur, when $\mu = 0$, at points with z coordinates z_i, z_{i+1}, etc., where the $\xi \ln z_i$ differ, asymptotically, by π. Furthermore, we may calculate the asymptotic ratio of the μ values, μ_i, μ_{i+1}, . . . , at which the curve of Fig. 3.2(ii) is vertical; we choose μ_i to be one such value and follow the curve up to the next such value to get μ_{i+1}, etc. [Thus, if $\mu_i > 0$ then $\mu_{i+1} < 0$, $\mu_{i+2} > 0$, etc.] The μ_i will be parameter values at which the left-hand side of Eq. (9) is tangential to the right-hand side of (9) at points z_i. For small enough z these tangencies occur nearly at the maxima and minima of the curve on the right side of (9) and the left side of (9) is approximately $z - \mu$. Maxima and minima of the right side of (9) occur at z values z_i, z_{i+1} with $|\xi \ln z_i - \xi \ln z_{i+1}| \approx \pi$ and so we get, using $z - \mu = \pm c z^{\delta}$ (some constant c) at fixed points occurring at such z values.

$$\frac{\mu_{i+1}}{\mu_i} = \frac{z_{i+1} + z_{i+1}^{\delta} c}{z_i - z_i^{\delta} c} \approx -\left[\frac{z_{i+1}}{z_i}\right]^{\delta} \approx -\exp\left[\frac{\pi\delta}{\xi}\right]$$

Remembering that $\delta = \lambda_2/\lambda_1$, and $\xi = \omega/\lambda_1$ we have

$$\lim_{i \to \infty} (\mu_{i+1}/\mu_i) = -\exp(-\pi\lambda_2/w) \tag{12}$$

If the quantity $\pi\lambda_2/\omega$ in this relation is large, we can expect the wiggles in Fig. 3.2(ii) to decrease in size very rapidly as period increases; in this case the difference between the $\delta < 1$ and the $\delta > 1$ approaches to homoclinicity may not be easily observed numerically and may not be particularly relevant from a global point of view.

3.1.3. Stability of Fixed Points. It is desirable to calculate some of the stability properties of the fixed points of (7) (and hence of the periodic orbits on which they lie). Our analysis is only partial, but tells us all we need to know. We may write the linear part of (7) as

$$\begin{bmatrix} r' \\ z' \end{bmatrix} = \begin{bmatrix} A & C \\ D & B \end{bmatrix} \begin{bmatrix} r \\ z \end{bmatrix}$$

where

$$\begin{aligned} A &= \alpha z^{\delta}\cos(\xi \ln z + \Phi_1) \\ B &= \beta r z^{\delta-1}\left[\delta\cos(\xi \ln z + \Phi_2) - \xi\sin(\xi \ln z + \Phi_2)\right] \\ C &= \alpha r z^{\delta-1}\left[\delta\cos(\xi \ln z + \Phi_1) - \xi\sin(\xi \ln z + \Phi_1)\right] \\ D &= \beta z^{\delta}\cos(\xi \ln z + \Phi_2) \end{aligned} \tag{13}$$

The eigenvalues of the matrix will be

$$\tfrac{1}{2}\left\{(A+B) \pm \left[(A+B)^2 - 4(AB-CD)\right]^{1/2}\right\} \tag{14}$$

It is clear that when $\delta > 1$ these eigenvalues will always be small in modulus if z is small (z^{δ} and $z^{\delta-1}$ will both be small). Thus the fixed point of (7) will be stable if it occurs with small z, and hence the one periodic orbit existing in $\mu > 0$ for $\delta > 1$ is stable for μ small enough.

The case $\delta < 1$ is a little more complicated. First notice that the determinant of the matrix, $AB - CD$, only contains terms of size $z^{2\delta-1}$. Thus, the map will be area contracting for $1 > \delta > 1/2$ and area expanding for $\delta < 1/2$, and we can expect different results in these two δ ranges. To obtain more information we look at two sets of z values (but always $z \ll 1$). These are those for which $B = 0$ or $D = 0$. The choice of these sets of z values is made because B and D contain the same trigonometric functions which appear in the right-hand side of the equation (9); that equation told us the z coordinates of the fixed points for various values of μ and δ and so the conditions $B = 0$ and $D = 0$ will be easily interpreted in terms of which fixed points are being considered. To be precise, the condition $B = 0$ is the same as the condition that the fixed point occur on a turning point of the right side of (9) (the wiggly curves in Fig. 3.1) and the condition $D = 0$ is the condition that the fixed point occur at a point where the curve crosses zero.

When $D = 0$ Eq. (14) reduces to a particularly simple form and we have eigenvalues A and B. Of these, A is always small (z^{δ} small) and B is always large ($z^{\delta-1}$ large—note $B \neq 0$ if $D = 0$). In particular, for $\mu = 0$ [$\delta < 1$; Fig. 3.1(v)] the fixed points of (7) occur with the condition $D = 0$ nearly satisfied for z small enough; this implies that the countably infinite collection of fixed points existing at these parameter values contains only saddle points.

When $B = 0$ the eigenvalues, (14), are $\{A \pm (A^2 + 4CD)^{1/2}\}$ and both eigenvalues will have large or small modulus depending on whether CD is large or small ($A^2 \sim z^{2\delta}$ can be neglected compared to $CD \sim z^{2\delta-1}$ and then, similarly, A can be neglected compared to $CD^{1/2}$). This, in turn, depends

on whether $\delta < 1/2$ or $\delta > 1/2$ ($CD \sim z^{2\delta - 1}$). Thus, $B = 0$ gives stable fixed points if $\delta > 1/2$ and unstable fixed points (sources) if $\delta < 1/2$.

At this point we return to consideration of Fig. 3.2(ii). If we examine how the system appears as we alter μ monotonically we observe μ values (an infinite number of them) on both sides of $\mu = 0$ at which a pair of periodic orbits appears or disappears. At each such μ value we have a saddle-node or tangent bifurcation, and, as is well known, such bifurcations produce (or destroy) either a stable/saddle pair of orbits or an unstable/saddle pair of orbits. We deduce, from above, that the former is the case when $1 > \delta > 1/2$ (at least for bifurcations occurring with μ small enough), and the latter the case when $\delta < 1/2$. There is one additional piece of information we require to complete the picture; that is, which of the orbits is stable ($\delta > 1/2$) or unstable ($\delta < 1/2$) and which a saddle. Figure 3.3 shows a blow-up of a part of the wiggly curve from Fig. 3.1 [which is the right-hand side of Eq. (9)] together with the left-hand side of (9) for seven different values of μ. These satisfy $\mu_1 > \mu_2 > \mu_3 > \mu_4 > 0 > \mu_5 > \mu_6 > \mu_7$. For $\mu = \mu_6$ we get the tangency and at $\mu = \mu_5$ we have two fixed points. From our analysis of the return map at fixed points we know that

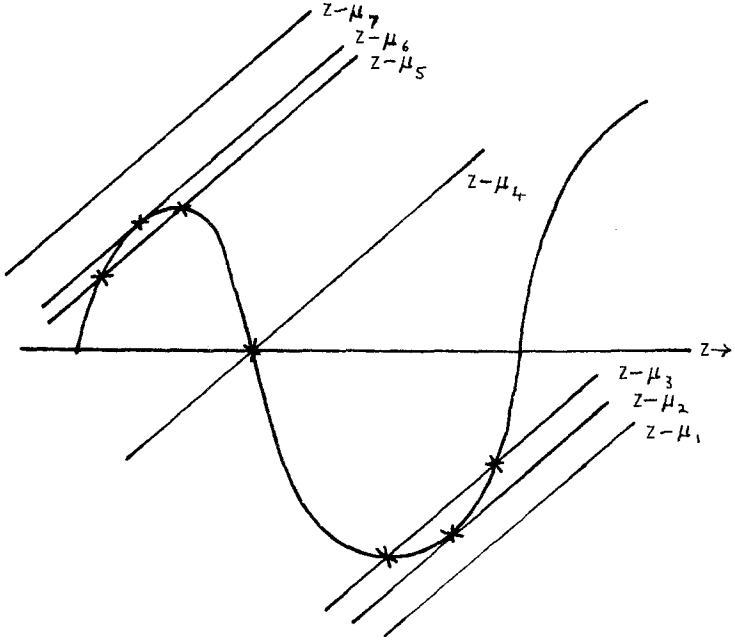

Fig. 3.3. Intersections of $z - \mu$ with a section of the curve given by the right-hand side of Eq. (9); $\mu_1 > \mu_2 > \mu_3 > \mu_4 > 0 > \mu_5 > \mu_6 > \mu_7$.

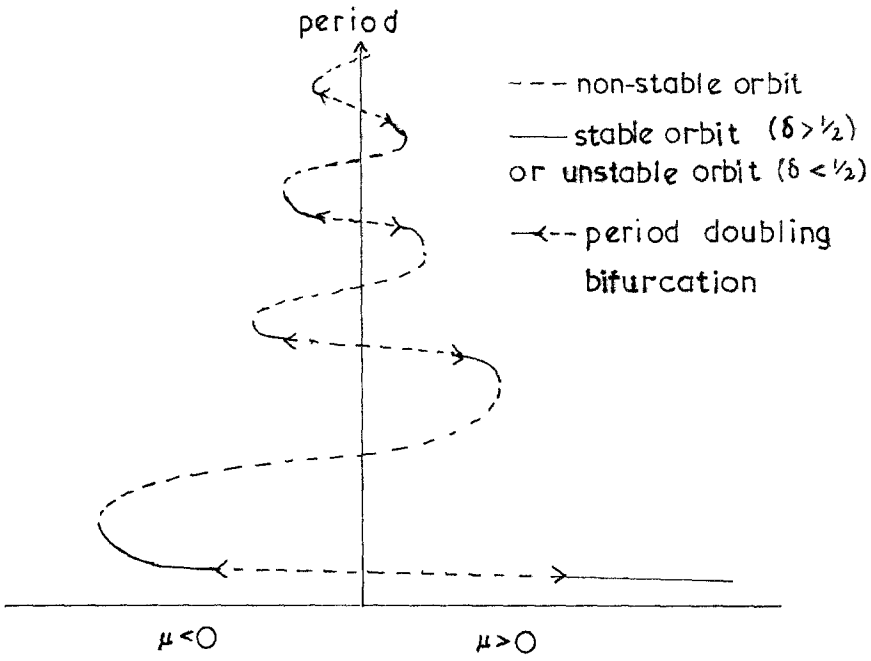

Fig. 3.4. Stability information for the bifurcation curve ($\delta < 1$) of Fig. 3.2(ii). The stable (unstable) sections of the curve appear, in examples, to be very short.

the fixed point at the maximum of the wiggly curve is the stable (unstable) one; the other must be the saddle. Of the two fixed points at $\mu = \mu_5$ it is the one with the larger z coordinate, i.e., the lower period, which is stable (unstable).

As we continue to increase μ into $\mu > 0$ we reach μ_4 where we know the fixed point is again a saddle. Clearly the fixed point has lost stability (unstability) in a period-doubling bifurcation. As μ increases to μ_3 we see that the fixed point, which again lies on a turning point of the wiggly curve, has become stable (unstable) again, and this restabilization must occur through a reverse period-doubling bifurcation. At $\mu = \mu_2$ we get the next saddle-node bifurcation and deduce that at this bifurcation (in $\mu > 0$) it is the orbit of higher period which is stable. This information allows us to redraw Fig. 3.3(ii) as in Fig. 3.4. We now have complete stability information for the curve shown.

3.2.4. Sil'nikov's Results. We have shown, explicitly, how a periodic orbit approaches homoclinicity in the two cases $\delta < 1$ and $\delta > 1$. This demonstration is, as far as we know, new, but the ideas and techniques behind it date back to Sil'nikov.[1,2] We have, by now, reproduced Sil'-

nikov's original results insofar as they relate to fixed points of the return map (7). These state that (a) for $\delta < 1$ and $\mu = 0$ there are a countable infinity of periodic orbits in a neighborhood of the homoclinic orbit, all of which are saddles, and (b) that for $\delta > 1$ there is one stable periodic orbit in a neighborhood of the unstable manifold of the stationary point in $\mu > 0$.

There are deeper implications of Sil'nikov's results and approach for the case $\mu = 0$, $\delta < 1$, which concern the complicated recurrent behavior, occurring near the homoclinic orbit, which is not represented by fixed points of (7) but by periodic or aperiodic points. For example, it is known that the invariant set of the return map (7) ($\mu = 0$, $\delta < 1$) contains one trajectory corresponding to each doubly infinite sequence of n symbols for any n however large; less precisely, the return map contains an infinite number of horseshoe maps (see, for example, Ref. 4 or 10). Intuitively and loosely, one may think of one horseshoe developing on each of the stable branches of the bifurcation curve shown in Fig. 3.4. In other words, on each of these branches we have not only the period-doubling bifurcations that destabilize and restabilize the periodic orbit represented by the curve of Fig. 3.4, but complete period-doubling cascades, and a countable infinity of other period-doubling cascades following or preceding saddle-node bifurcations, leading to a full horseshoe map at $\mu = 0$. A recent paper by Yorke and Alligood[11] outlines a proof of a theorem stating that, in certain circumstances, infinitely many cascades of period-doubling bifurcations must occur in the formation of a horseshoe. This result gives something of the flavor of the situation leading up to homoclinicity at $\mu = 0$ but cannot, in fact, be applied directly here; our situation is much more complicated due, in part, to the existence of infinitely many homoclinic orbits in addition to the principal one discussed so far (see below) and, in part, to the fact that the invariant set of (7) contains periodic orbits and trajectories which communicate between horseshoes—we may not properly consider the developments on each branch of Fig. 3.4 separately, at least for the large period branches.

All of these results do not, in general, contribute much to our understanding of numerical results, or to our understanding of how the complicated series of bifurcations occurring near a homoclinicity fits into more global bifurcation pictures. Consequently we do not dwell on them. We will see, though, that our simpler considerations below give considerable insight into the more complicated structures.

3.2. Subsidiary Homoclinic Orbits

When $\mu > 0$ it is possible that the unstable manifold of the origin, after one or more close encounters with the stationary point which pass off without homoclinicity being achieved, will eventually arrive back in the

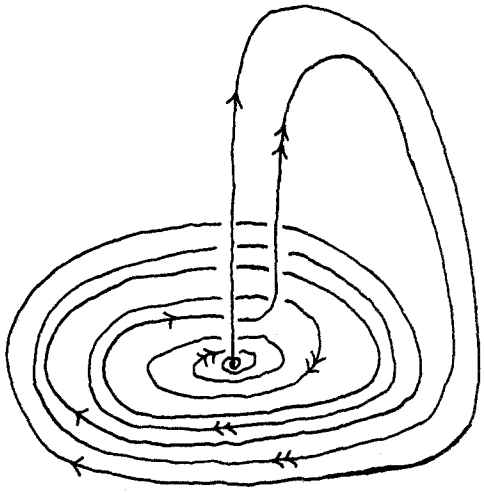

Fig. 3.5. A double pulse subsidiary homoclinic orbit which passes only once near the stationary point without achieving homoclinicity.

linear region of our analysis with $z = 0$ and from there spiral back into the stationary point. In other words, we may have more complicated homoclinic orbits than the one which occurs at $\mu = 0$. If such exist we shall call them *subsidiary homoclinic orbits*. The homoclinic orbit at $\mu = 0$ we call the *principal homoclinic orbit*. We examine only the simplest possible subsidiary homoclinic orbits, occurring when the unstable manifold of the stationary point has only one unsuccessful encounter with the stationary point before achieving homoclinicity. The situation we hope to find is shown in Fig. 3.5, which, we have recently discovered, has also been studied by Gaspard[12] using techniques almost identical to those described here. In addition, Hastings[13] discusses the existence of such orbits in a particular three-dimensional system whose solutions represent traveling waves in the Fitz-Hugh–Nagumo model of nerve conduction; he calls them "double-pulse" solutions, and we shall use this term to distinguish these orbits from other, more complicated subsidiary homoclinic orbits. See also Refs. 14 and 15.

The unstable manifold first arrives back in our linear region with coordinates $(\bar{r} + a\mu, \mu)$. For $\mu > 0$ Eq. (7) gives us, for the next return, a z coordinate

$$\mu + \beta(\bar{r} + a\mu)\,\mu^{\delta}\cos(\xi \ln \mu + \Phi_2)$$

If this coordinate is zero, we have located the homoclinic orbit we require; if it is positive the next return is defined and we may have more complicated homoclinic orbits occurring after more passages through the linear

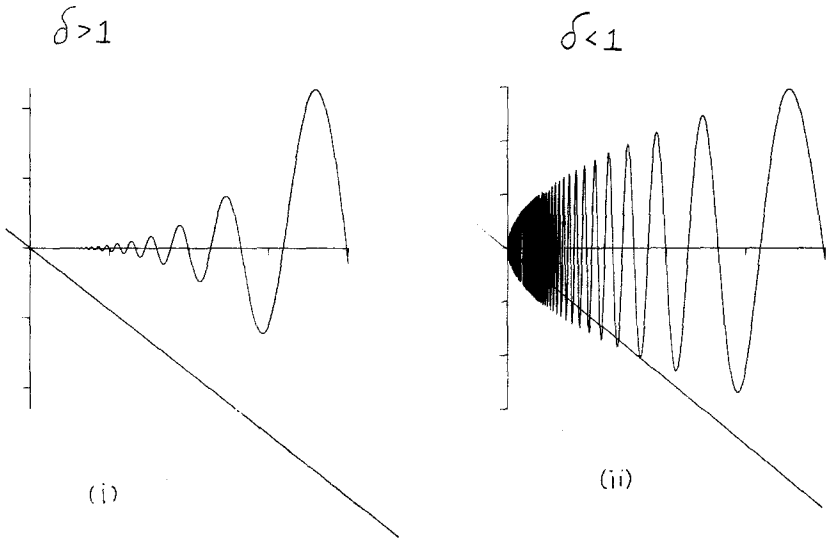

Fig. 3.6. Two curves, $-\mu$ and $\beta(\bar{r}+a\mu)\mu^{\delta}\cos(\xi \ln \mu + \Phi_2)$, which are the left and right sides of Eq. (15). Intersections of the curves give the μ values at which double pulse subsidiary homoclinic orbits occur. (i) $\delta > 1$; (ii) $\delta < 1$.

region; if it is negative the trajectory wanders off and is of no further interest. The critical condition is given, therefore, by

$$-\mu = \beta(\bar{r}+a\mu)\,\mu^{\delta}\cos(\xi \ln \mu + \Phi_2) \tag{15}$$

We treat this equation in the same way we treated Eq. (9). Figure 3.6 shows the two curves representing the left and right sides of (15) for $\delta > 1$ and $\delta < 1$, and the intersections give the homoclinic orbits we require. In $\delta > 1$ there are no such intersections for μ small, though there may be some at larger μ particularly if δ is close to one. When $\delta < 1$ we have a countable infinity of such intersections for small μ, and those occurring at smaller μ are the ones which represent homoclinic orbits which spiral round more times on the first passage through the linear region (cf. the arguments of Section 3.1.2). Gaspard[12] shows that successive double-pulse subsidiary homoclinic orbits occur at μ values μ_i, μ_{i+1}, etc. which are related asymptotically by $\mu_{i+1}/\mu_i = \exp(-\pi\lambda_1/\omega)$. This result may be obtained in almost exactly the same way that we obtained the asymptotic relation (12) in Section 3.1.2. Notice that if $\pi\lambda_1/\omega$ is large these orbits may be hard to observe numerically and that we have $\delta < 1$ which implies $\pi\lambda_1/\omega$ is large if $\pi\lambda_2/\omega$ [from (12)] is large.

Notice, also, that Fig. 3.6 suggests that the intersections we get come in pairs; in other words, for a particular value of δ, and for a particular

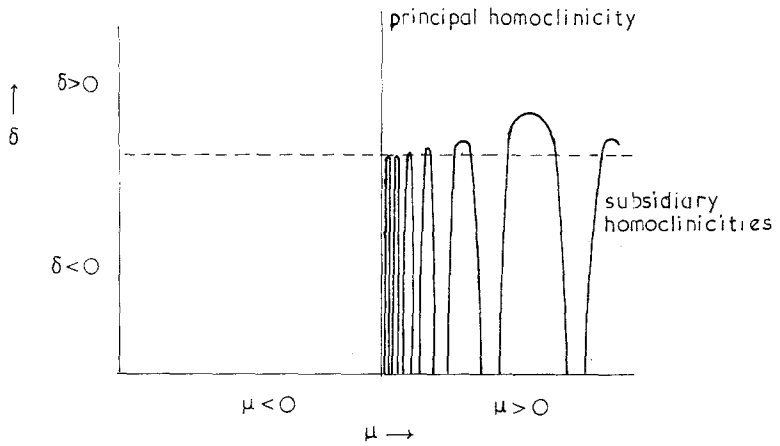

Fig. 3.7. Curves in a two-parameter space (μ, δ) showing parameter values at which we have homoclinic orbits. Only double pulse homoclinic orbits are drawn. There are an infinity of hooped curves accumulating on $\mu = 0$. The curves may or may not encroach into $\delta > 1$ for $\mu > 0$.

interval of μ values such that $\xi \ln \mu$ varies over 2π, we either get no intersections or two (excluding the possibility of a tangency). This, in turn, suggests that we can draw Fig. 3.7 which must be interpreted differently from previous figures in this paper. In Fig. 3.7 we have drawn a two-dimensional parameter space: μ is one parameter but we now assume that we can change the system so that δ varies also (but always with principal homoclinicity at $\mu = 0$). The curves of Fig. 3.7 represent parameter values at which homoclinic orbits occur. The vertical line gives principal homoclinicity for all δ at $\mu = 0$. The other curves represent homoclinicities of the kind discussed above, i.e., homoclinic orbits represented by solutions of (15).

Figure 3.7 is very schematic, and actually we want to be able to draw an infinity of hooped curves accumulating on $\mu = 0$. The tops of the hoops should accumulate at $\mu = 0$, $\delta = 1$. This picture then agrees with the results above; if μ is increased from zero at fixed $\delta > 1$, a finite number of curves at finite μ values are crossed, and if μ is increased from zero at fixed $\delta < 1$, a countable infinity of curves at arbitrarily small μ values are crossed.

It would be interesting to speculate on the likely position of additional curves which could be drawn on Fig. 3.7 to represent even more complicated homoclinic orbits (those occurring after $2, 3, 4, \ldots$ nonhomoclinic passes through the linear region) but we refrain from doing so here. Note, however, that all such curves lie outside the hoops of Fig. 3.7 [because the space inside the hoops is that for which $-\mu > \beta(\bar{r} + a\mu)\mu^{\delta}\cos(\xi \ln \mu + \Phi_2)$

—see the remarks above Eq. (15)] and that curves may not cross since only one kind of homoclinicity can occur at any particular set of μ, δ values.

3.3. Predictions for Global Behavior

Our major concern in this paper is to show how the local results obtained above fit into global bifurcation pictures. Before considering actual examples, there are some predictions we can make on the basis of the return map (7) and of our work so far. We first consider the behavior of numerically calculated trajectories near to principal homoclinicity, and then consider what we are likely to see in two-parameter systems where we can change both μ and δ.

3.3.1. The Behavior of Most Trajectories near Homoclinicity. When $\delta > 1$, trajectories calculated numerically appear to behave as we would expect. In other words, for $\mu > 0$ they appear to be attracted to the stable periodic orbit which is approaching homoclinicity, and for $\mu < 0$ (when the analysis predicts no periodic orbits) they rapidly arrive on the wrong side of the stable manifold of the stationary point and disappear (to infinity in the example of Section 4.2). This can be understood by looking at the z coordinate of the return map (7). For large δ trajectories will tend to return to the linear region with z coordinate near μ; thus, if μ is positive they go round again, and if μ is negative they are lost. When $\delta < 1$, and despite the large number of stable orbits predicted by the analysis, most trajectories appear to be lost fairly rapidly. Again, the z coordinate of (7) shows why this should be. The cosine term multiplied by z^{δ} is now likely to be relatively large and many trajectories will return to the linear region with $z < 0$, even if $\mu > 0$. It is perhaps worth mentioning here that our experience of examples is that the stable orbits predicted on alternate branches of the bifurcation curve for the principal periodic orbit (Fig. 3.4) exist only for very short parameter intervals, even when the total length of the whole branch is relatively large. Presumably the same applies, except more so, to more complicated periodic orbits and to stable chaotic motions that might be predicted by the analysis. To conclude, we expect most trajectories to be lost for μ near zero if $\delta < 1$. [Note, however, that we can expect to see bounded motions near to homoclinicity if we have a symmetry such as that shown in Fig. 2.3(a); we are not considering that case here.]

3.3.2. Local and Global Bifurcation Pictures. The analysis so far has been concerned mainly with Eq. (7) for r, z, and μ very small, and δ definitely greater or less than one. It is interesting and useful to notice that if we consider (7), (9), and (16) for larger r, z, and μ values, and for δ close to one, we can see how a system could move smoothly from the $\delta > 1$ to

the $\delta < 1$ case. We do not consider this in detail, but Fig. 3.8 shows plausible bifurcation curves for the principal periodic orbit which could be extracted from Eq. (9) with suitable choices for the parameters a, α, β, Φ_1, Φ_2, and δ.

Notice that in all the diagrams of Fig. 3.8 we can select a parameter interval, $|\mu| < \epsilon$, such that outside this interval the only periodic orbit in existence is a single stable periodic orbit. There may be many situations when we will be justified, from a global point of view, in ignoring the details of what happens near to homoclinicity, and thinking of this principal periodic orbit as being the only product of the whole series of bifurcations which occurs near to homoclinicity. We shall see, when we examine examples, that this point of view can be useful. In particular, we find it useful in three slightly different cases, all of which can be expected to occur frequently in a wide variety of systems.

(i) A system may be of interest primarily because of some sequence of bifurcations other than those associated with a homoclinicity of the type

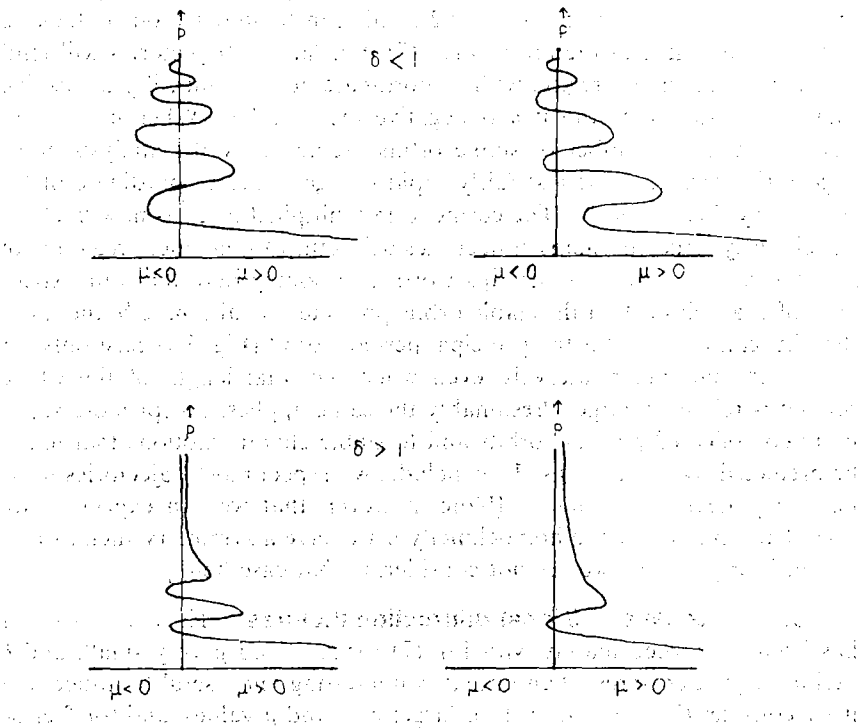

Fig. 3.8. Possible results of considering Eqs. (7), (9) outside the region $z, \mu \ll 1$. We can expect bifurcation curves such as those shown here in numerical examples, particularly if δ is near one.

discussed here. In that case, we may want to know how many orbits our type of homoclinicity contributes to the other sequence of bifurcations. The answer, it seems, will often be just the one principal orbit which, we should notice, will be stable (or unstable) if it emerges from the interval $|\mu| < \epsilon$ into $\mu > 0$ (as in Fig. 3.8) but which will be nonstable (a saddle) if it emerges into $\mu < 0$ (which is also possible). In this kind of case our one-orbit point of view may be useful even if the parameter interval $|\mu| < \epsilon$ is relatively large (cf. Section 4.1).

(ii) Experience suggests that many systems of equations have very similar global bifurcation pictures and very similar sequences of numerical behavior changes. If we desire to describe one of the frequently occurring bifurcation patterns that involves complicated sequences of homoclinic orbits, we will not wish to be distracted from the general picture by such details as exactly which homoclinic orbits occur with $\delta < 1$ and which with $\delta > 1$. In such cases the one-orbit point of view is very useful for blurring over the complications consequent on thinking of $\delta < 1$ and $\delta > 1$ as two quite distinct cases, and is often easily justified in the sense that the relevant parameter intervals, $|\mu| < \epsilon$, are very small (cf. Sections 4.2 and 4.3).

(iii) In some systems with bifurcation curves like those shown in Fig. 3.4 or 3.8, we find that the parameter distance between the two period-doubling bifurcations occurring on the lowest branch of the bifurcation curves is an order of magnitude larger than the length of a parameter interval needed to cover all the rest of the behavior near to homoclinicity. This occurs, in particular, when the quantities $\pi\lambda_2/\omega$ and $\pi\lambda_1/\omega$ are small at homoclinicity as explained in Sections 3.1.2 and 3.2. In these cases almost all of the numerically observed behavior is due to bifurcations associated with the lower branch and there are good reasons for considering this sequence of bifurcations separately from the rest of the behavior changes associated with the principal homoclinicity. Foremost amongst these reasons is the observed fact that much of the behavior associated with the lowest branch occurs far from principal homoclinicity and in regions of phase space far from the homoclinic orbit. Thus, even if the bifurcations which are observed seem to fit into a pattern compatible with patterns predicted by the local analysis for higher branches of the bifurcation curve of the principal periodic orbit, we maintain that it is not sensible to claim that they can be properly predicted by the local analysis; in addition, it is on the lowest branch that deviations from the behavior predicted by the local analysis are most likely to occur. In some systems numerically observed behavior may be due to bifurcations occurring on several branches of the principal bifurcation curve (Figs. 3.4 or 3.8) at once, but in the situation described above we find it useful to think of principal homoclinicity as producing just one periodic orbit, which then undergoes a series of bifurcations which we study separately.

Before proceeding to study examples, it is worth making some final remarks about the local analysis in the light of the remarks above. In Section 3.2 we showed the existence of an infinity of subsidiary homoclinic orbits in $\mu > 0$ when $\delta < 1$. Clearly, we could analyze each of these homoclinicities in the same way that we analyzed the principal homoclinic orbit, gaining, in the process, some idea of the deep levels of self-similarity inherent in the bifurcation structure near a principal homoclinic orbit. More immediately, we can ignore the details of the bifurcations occurring near to a subsidiary homoclinic orbit and suppose, in the spirit of the remarks above, that each contributes just one periodic orbit to the local bifurcation picture of the principal homoclinicity. Remembering that subsidiary homoclinic orbits occur in pairs (Section 3.2 and Fig. 3.7) there are two obvious possibilities for the way in which these orbits enter the local picture, both illustrated in Fig. 3.9. Figure 3.9(i) shows the situation which we believe exists for the double-pulse subsidiary orbits described in Section 3.2; each pair of subsidiary homoclinicities produces a pair of orbits which utimately diverge (in parameter space), each going to one of the period doublings occurring on a branch of the principal periodic orbit's bifurcation curve. It seems likely that the two orbits go off in different directions in parameter space because if we define two new parameters, μ_1 and μ_2, which are zero at the two subsidiary homoclinicities, respectively, then in analogy with our analysis of the principal homoclinicity (see Fig. 2.1) we will have both μ_1 and μ_2 less than zero in the μ interval between the two subsidiary homoclinicities and, in general, we expect the one orbit "produced" by a homoclinicity to exist in the region $\mu > 0$. We expect these

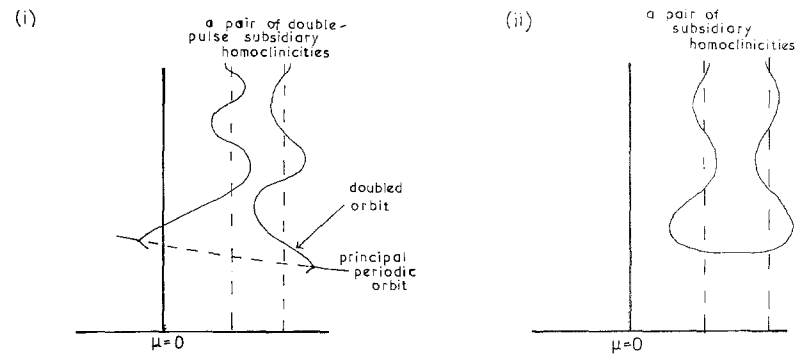

Fig. 3.9. Bifurcation curves for the periodic orbits produced by subsidiary homoclinic orbits ($\delta < 1$). (i) Conjectured bifurcation diagram for double pulse subsidiary homoclinic orbits. (ii) It is possible that a pair of orbits produced by a pair of subsidiary homoclinic orbits join up; this is considered unlikely for the double pulse orbits (see text).

orbits to join up with the period-doubled orbits from the principal bifurcation curve by analogy with the numerical results of Section 4.2 on the lowest branch of the principal curve; this also seems reasonable if we attempt to match up orbits with similar amounts of spiralling near the stationary point. Figure 3.9(ii) shows the other obvious possibility, where the two orbits just join up; this may well occur for some of the more complicated subsidiary orbits which we have not examined, even if it is never correct for double-pulse subsidiaries.

4. EXAMPLES

In this section we will study three examples of systems of ordinary differential equations having, for some parameter values, homoclinic orbits of the type analyzed in previous sections. The numerical experiments reported below were all done using standard integrating packages. The technique used to follow periodic orbits with changing parameters is similar to that described by Sparrow,[16] but the bifurcation curves which involve following orbits through several saddle-node bifurcations were obtained by adapting that technique so that it searched for new positions of the orbit using a fixed increment in period rather than a fixed increment in parameter.

4.1. The Lorenz Equations

The Lorenz equations[17] are a well-known system of differential equations displaying a variety of different chaotic behaviors. The equations

$$\begin{aligned} \dot{x} &= \sigma(y - x) \\ \dot{y} &= rx - y - xz \\ \dot{z} &= xy - bz \end{aligned} \tag{16}$$

are usually studied for parameter values $\sigma = 10$, $b = 8/3$, and $0 < r < \infty$, for which values our previous discussion is irrelevant. However, it is argued in Ref. 16 that for small enough b values (or large enough σ values) there will be symmetric heteroclinic orbits between the two stationary points $(\pm[b(r-1)]^{1/2}, \pm[b(r-1)]^{1/2}, r-1)$ for some r value. When $\sigma = 10$, small enough b appears to include all of $b < b^*$ for some $2 < b^* < 8/3$, and for $\sigma = 10$, $b = 0.25$, the relevant r value appears to be $r^* \approx 487.16$. At these parameter values the eigenvalues of the linearized flow near the two stationary points are approximately -14.371 and $1.560 \pm 12.912i$ and we have, therefore, if we *reverse the direction of the flow*, the situation shown in Fig. 2.3. Notice that the equations (16) have the symmetry $(x, y, z) \to (-x, -y, z)$, implying that the heteroclinic connections (which occur when

one branch of the one-dimensional stable manifold of each point is included in the two-dimensional unstable manifold of the other point) occur simultaneously as shown in the symmetric Fig. 2.3.

The analysis of our previous sections will apply to this situation, with obvious adjustments to cope with the symmetry, if we consider the Lorenz equations in *reverse time*. (The direction of the flow will make no difference to topological results, e.g., the existence of periodic orbits, but it will affect stability considerations.) The relevant parameters from the previous analysis will be $\delta \approx 0.108$, ($\delta < 1/2$), and $\mu > 0$ of previous sections corresponds with the parameter range $r > r^*$ as can be seen from Fig. 4.1. Figures 4.1(i) and 4.1(iv) show both branches of the stable manifold of the stationary point which lies in $x > 0$ at parameter values relatively far from homoclinicity.

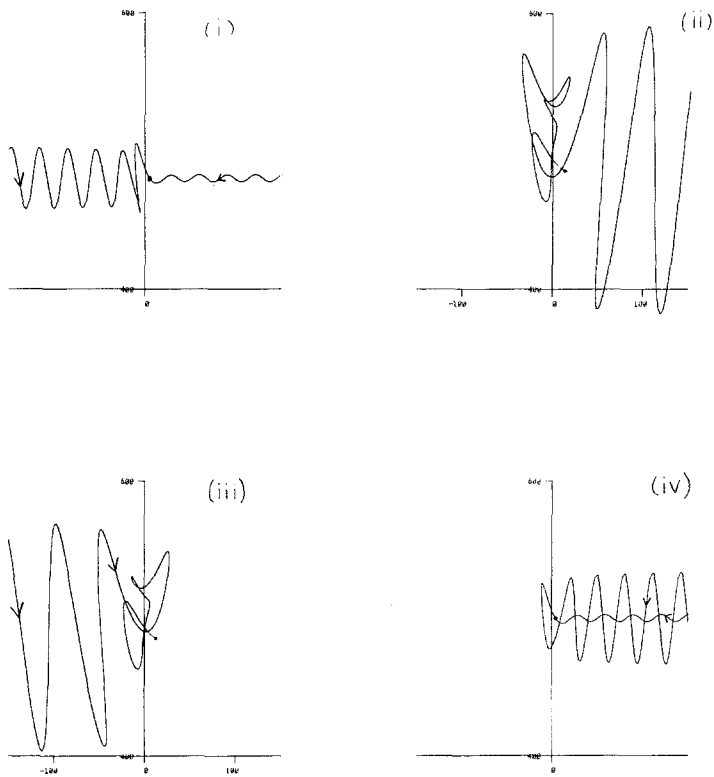

Fig. 4.1. The stable manifold of the stationary point in $x > 0$ (calculated by integrating the equation backwards in time). (i) $r = 480.0$, both branches; (ii) $r = 487.23$; (iii) $r = 487.25$; (iv) $r = 500.0$ both branches.

The branch which oscillates less fiercely goes straight out to infinity in the same direction on both sides of the bifurcation (cf. $z < 0$ in Section 2) so it is the fiercely oscillating branch which interests us. Since, in Fig. 4.1(i), this branch tends to infinity in the same direction as the less fiercely oscillating branch of the other stationary point (remember the symmetry) it is clear that Fig. 4.1(i) corresponds to the case $\mu < 0$. The principal symmetric heteroclinic connection occurs at $r^* \approx 487.16$ and a series of subsidiary homoclinic or heteroclinic connections can be seen to occur in $r > r^*$ as the fiercely oscillating branch of the stable manifold changes its behavior and tends alternately to $\pm\infty$. Principal heteroclinicity occurs between Fig. 4.1(i) and Fig. 4.1(ii), and subsidiary connections occur between Figs. 4.1(ii) and 4.1(iii) and between Figs. 4.1(iii) and 4.1(iv). Many other direction changes can be also observed with relative numerical ease.

We will concentrate here on the simplest orbits occurring near $r = r^*$, but notice the following correspondences between the analysis of Section 3 and the results of a full analysis for the symmetric system:

i. Fixed points of the nonsymmetric analysis will give symmetric periodic orbits of the symmetric system.

ii. Periodic points of odd period in the nonsymmetric analysis will also give symmetric orbits in the symmetric system.

iii. Periodic points of even period in the nonsymmetric analysis will give symmetric pairs of nonsymmetric orbits in the symmetric system.

Similar correspondences will occur between the more complicated (subsidiary) homoclinic orbits occurring in the nonsymmetric analysis and either more complicated (subsidiary) symmetric heteroclinic connections or symmetric pairs of homoclinic connections in the symmetric system. Here we look only at the orbits corresponding to fixed points of the nonsymmetric analysis. Hence we are going to look at certain symmetric orbits occurring in the Lorenz system.

Figure 4.2 shows a bifurcation curve, calculated numerically, for the principal symmetric orbit. This is a stunning example of the $\delta < 1$ approach to homoclinicity; we only stopped following the curve of Fig. 4.2 because the wiggles were getting very small, not because there were numerical problems with going further. Figure 4.3 shows the orbit in question at the three points marked (*), (**), and (***) on Fig. 4.2. As explained in Section 3.1.2, the orbit "winds itself up" about the stable manifolds of the stationary points as we follow the bifurcation curve back and forth. Observe that our various calculations concerning the shape of the bifurcation curve (Section 3.1.2) give answers compatible with the numerically calculated curve in Fig. 4.2. Thus, the period of the orbit at successive intersections of the curve with $r = r^*$ increases by an approximately constant amount

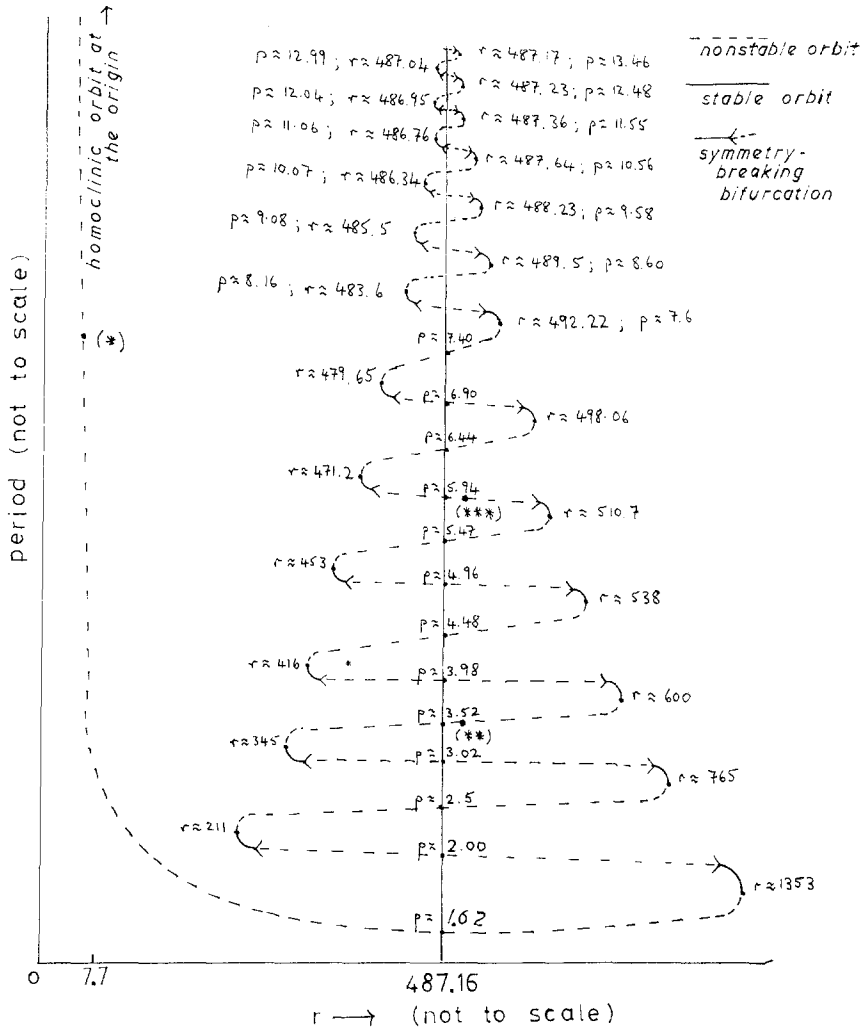

Fig. 4.2. Bifurcation curve for the symmetric principal orbit in the Lorenz equations (not to scale). $b = 0.25$, $\sigma = 10.0$. The orbit is produced in a homoclinic "explosion" involving the stationary point at the origin, and disappears in the heteroclinic bifurcation involving the other two stationary points. The orbit is illustrated at (*), (**), and (***) in Fig. 4.3.

[$\pi/\omega \approx 0.244$, Eq. (11) of Section 3.1.2; we need $2\pi/\omega$ since the nonsymmetric analysis looks at only half of the orbit], and, at the accuracy we have used, the parameter distance between successive saddle-node bifurcations is tending to a constant ratio [$\exp(-\pi\lambda_2/\omega) \approx 0.684$, Eq. (12) of Section 3.1.2]. This ratio is reasonably near unity and the size of the oscillations in Fig. 4.2 decreases only slowly.

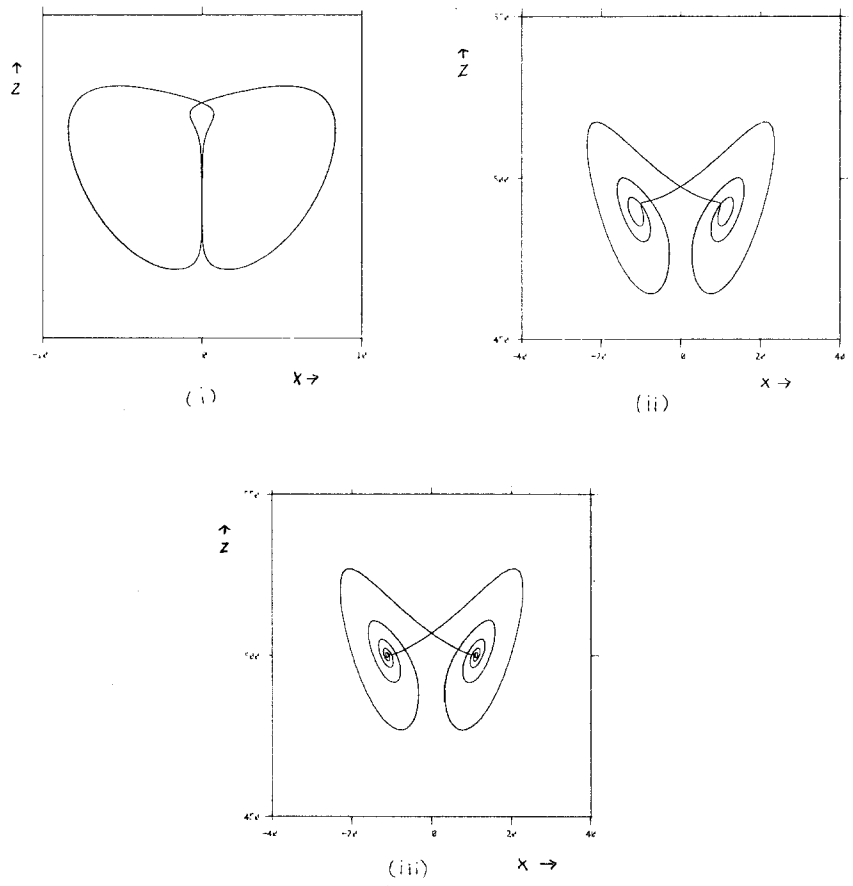

Fig. 4.3. The orbit from Fig. 4.2 illustrated at points (*) $r = 26.0$, period ≈ 7.0; (**) $r = 490.0$, period ≈ 3.52; (***) $r = 501.0$, period ≈ 6.0.

When we come to consider the stability of the orbits our numerically observed results also agree with the results of Section 3.1.3. In this case, however, we have an additional theoretical consideration which we can bring to bear. It is well known that the Lorenz equations have a constant negative divergence ($= -\sigma - b - 1$) and hence that there can be no totally unstable (source) objects (stationary points, periodic orbits, strange invariant sets, etc.) in the flow. This implies that there can be no stable (sink) objects in the reversed time Lorenz equations to which the analysis of Section 3 applies. Since we have $\delta < 1/2$ this result is not unexpected (Section 3.1.3); each of the saddle-node bifurcations in the reversed time Lorenz flow involves one saddle and one unstable orbit. Note also that we have the bifurcating branches of Fig. 4.2 going from $r > r^*$ ($\mu > 0$) to

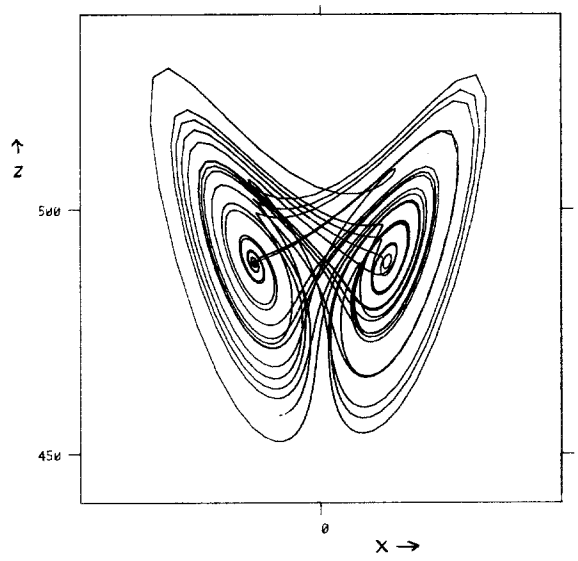

Fig. 4.4. Chaotic behavior near heteroclinicity. $r = 490.0$.

$r < r^*$ ($\mu < 0$) as period increases. This agrees with Section 3.1.3 and Fig. 3.4.

It is interesting to note that despite the large number of stable orbits expected for $r \approx r^*$ in the forward time Lorenz system, typical trajectories calculated numerically at r values near r^* do not appear to be attracted to any of them; though trajectories spend a considerable amount of time close to the heteroclinic orbits (as shown in Fig. 4.4), they repeatedly escape from this region and are only reinjected by other parts of the global flow after wandering far from the region of validity of any local analysis of the heteroclinic bifurcation. For more details of the global flow at these parameter values see Ref. 16; it appears that much of the global flow can only be understood in terms of homoclinic bifurcations associated with the stationary point at the origin (which we have not considered here and which has three real eigenvalues) and can definitely not be deduced from local analyses of the heteroclinic orbits. This wandering behavior is not, however, unexpected. Regardless of the direction of the flow and the stability of the orbits, we expect most trajectories eventually to move away from the region of local analysis (cf. Section 3.3.1) and in the case of the Lorenz equations (forward time) the dissipative nature of the flow, which ensures that all trajectories remain within a bounded region, seems to ensure that most typical trajectories are reinjected into the region of the local analysis after visiting other parts of phase space.

Before leaving the Lorenz equations, one further remark is in order. In Ref. 16 (Chapter 8) the occurrence of the heteroclinic connections was deduced after consideration of some relatively complicated conjectures about a global bifurcation picture for parameter values $\sigma = 10$, $b = 0.25$, and $0 < r < \infty$. These considerations led to the conclusion that there was one periodic orbit of a certain type which must be involved in some bifurcation other than the well-known homoclinic bifurcations at the orgin, period-doubling, saddle-node bifurcations etc. This orbit was the one illustrated in Figs. 4.2 and 4.3, and Sparrow[16] did conclude that the orbit eventually disappeared from the global bifurcation picture in a bifurcation involving heteroclinic orbits like those discussed here. The other side of these arguments (which appear reliable, though conjectural) is that the heteroclinicity discussed here contributes only this one orbit to the global bifurcation picture. In other words, for r outside a large enough r interval about r^*, the combined effect of the bifurcations discussed here (principal heteroclinicity, subsidiary homoclinic, and heteroclinic orbits etc.) is to add one and only one orbit to the global picture. This argument (which we cannot give in full here) adds plausibility to the remarks in Section 3.3.2, even though the relevant r interval is rather large ($211 < r < 1353$). Notice that the orbit is injected into the global picture in $r < r^*$ ($\mu < 0$), and hence is nonstable (a saddle).

[N.B. This paper, where it contradicts Ref. 16, is to supercede that work. In particular, and as is argued here, the subsidiary homoclinic and heteroclinic bifurcations occur on only one side ($r > r^*$) of the principal heteroclinic connection, and not on both sides as stated in Ref. 16.]

4.2. An Example from Arneodo *et al.* (Ref. 3)

4.2.1. Introduction. Arneodo *et al.*[3] investigate the ordinary differential equations

$$\dddot{x} + \ddot{x} + b\dot{x} - cx + x^2 = 0 \tag{17}$$

which they derive from normal form theory near a tricritical bifurcation. Equation (17) can be written as three coupled first-order differential equations:

$$\begin{aligned} \dot{x} &= y \\ \dot{y} &= z \\ \dot{z} &= -z - by + cx - x^2 \end{aligned} \tag{18}$$

The divergence of (18) is -1, so there are no completely unstable trajectories (otherwise the flow would be locally expansive); all periodic orbits are either stable or saddles. Arneodo *et al.*[3] have observed chaotic trajectories

at some values of the parameters b and c, and they have also located homoclinic orbits. Thus (18) provides us with an opportunity to confirm the local analysis of Section 3.

Following Arneodo *et al.*[3] we shall work in the region of parameter space with $b, c > 0$ (see Fig. 4.5, which is taken from Ref. 3) and compute bifurcation sequences with b fixed and c increasing. Arneodo *et al.*[3] investigated $b = 0.5$, 0.8, and 2.0; we use these lines and also $b = 1.5$. Many of our results were known to Arneodo *et al.*, but we are able to explain our observations in terms of the local analysis of Section 3 and incorporate them into a global bifurcation picture.

The system (18) has two stationary points: the origin, O, ($x = y = z = 0$) and B ($x = c$, $y = z = 0$). We shall be interested principally in the origin, which plays the role of the stationary point in Sections 2 and 3. For $c > 0$ the origin is always nonstable. Outside the cusplike region near the origin of parameter space in Fig. 4.5, the linearized flow at the origin has a complex conjugate pair of eigenvalues and one real eigenvalue. When $c > 0$ the real eigenvalue is positive and the real part of the complex conjugate pair of eigenvalues is negative. The ratio δ of the real parts of the

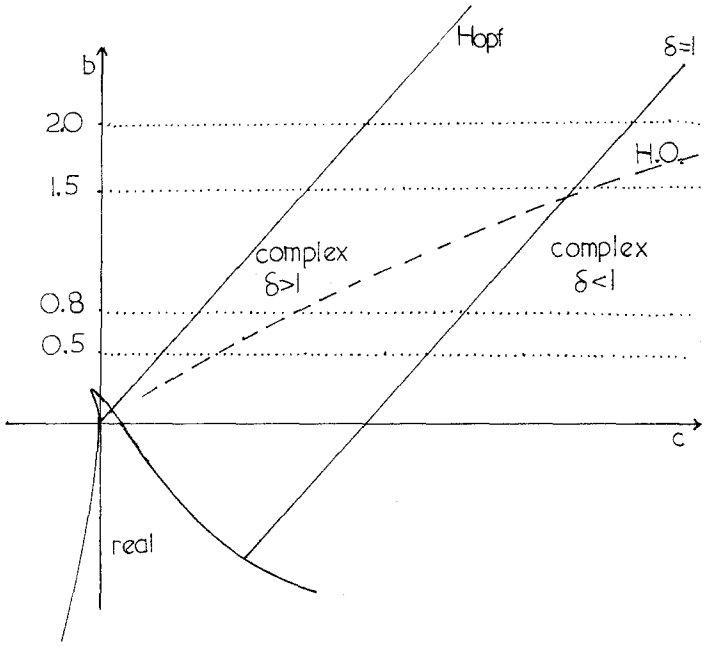

Fig. 4.5. (b, c) parameter space of (18) showing the eigenvalues at the origin, the locus of a homoclinic orbit to the origin, HO, and the locus of the Hopf bifurcation from B.

eigenvalues is unity along the line marked $\delta = 1$ in Fig. 4.5 given by

$$\begin{aligned} b &= c - 2 \\ c &> -1 \end{aligned} \tag{19}$$

Homoclinic orbits occurring for parameter values to the left of this line (i.e., small c) have $\delta > 1$ and homoclinic orbits occurring for parameter values to the right of this line (i.e., large c) have $\delta < 1$. The locus of a homoclinic orbit found by Arneodo *et al.*[3] is also shown in Fig. 4.5; it intersects the line $\delta = 1$ at $b = b_1 \approx 1.375$, $c = c_1 \approx 3.375$. Therefore, as we vary c with b fixed we will find the homoclinic orbit in the region of parameter space with $\delta > 1$ if $b < b_1$ (and hence for $b = 0.5$ and 0.8) and with $\delta < 1$ if $b > b_1$ (and hence for $b = 1.5$ and 2.0).

For fixed b, suppose the homoclinic orbit occurs at $c = c_b$. Then in the terminology of Section 3, $\mu = 0$ when $c = c_b$ (this is the condition for homoclinicity), $\mu > 0$ corresponds to $c < c_b$ and $\mu < 0$ corresponds to $c > c_b$. This observation will be important when we come to compare our results with the predictions of Section 3.

The second stationary point, B, is stable for $0 < c < b$ but (see Fig. 4.5) loses stability when $c = b$ in a supercritical Hopf bifurcation which creates an initially stable periodic orbit. We shall call this orbit the *principal periodic orbit* since, as we shall see, it corresponds to the homoclinic-related definition of principal periodic orbit given in Section 3.1.2.

4.2.2. The Approach to Homoclinicity. Numerical experiments indicate that the principal periodic orbit born in the Hopf bifurcation at

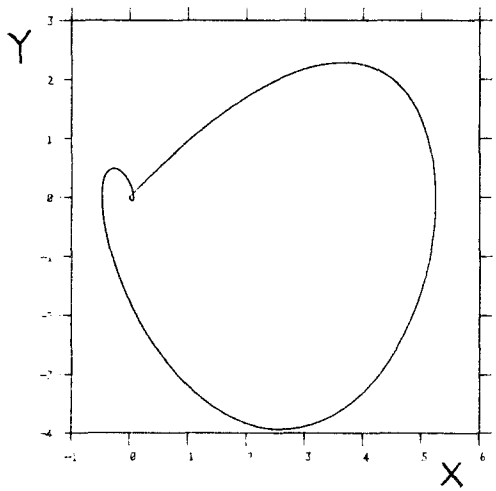

Fig. 4.6. The principal homoclinic orbit (approximately); $b = 1.5$, $c = 3.76113$.

$c = b$ is, in fact, the orbit which eventually forms the principal homoclinic orbit of Fig. 4.5. This orbit is shown, for $b = 1.5$, in Fig. 4.6.

Figure 4.7 shows the period of the principal periodic orbit as it is followed with changing c at the four fixed b values investigated. Figure 4.7 should be compared with Figs. 3.2, 3.4, and 3.8 which illustrate the predictions of Section 3.

We have not followed any orbit far enough to confirm all the quantitative results of Section 3.1.2; $\exp(-\pi\lambda_2/\omega)$, the factor which controls the convergence of the wiggles when $\delta < 1$, is small (0.136 for $b = 1.5$ and 0.157 for $b = 2.0$) so the width of the wiggles becomes small very quickly.

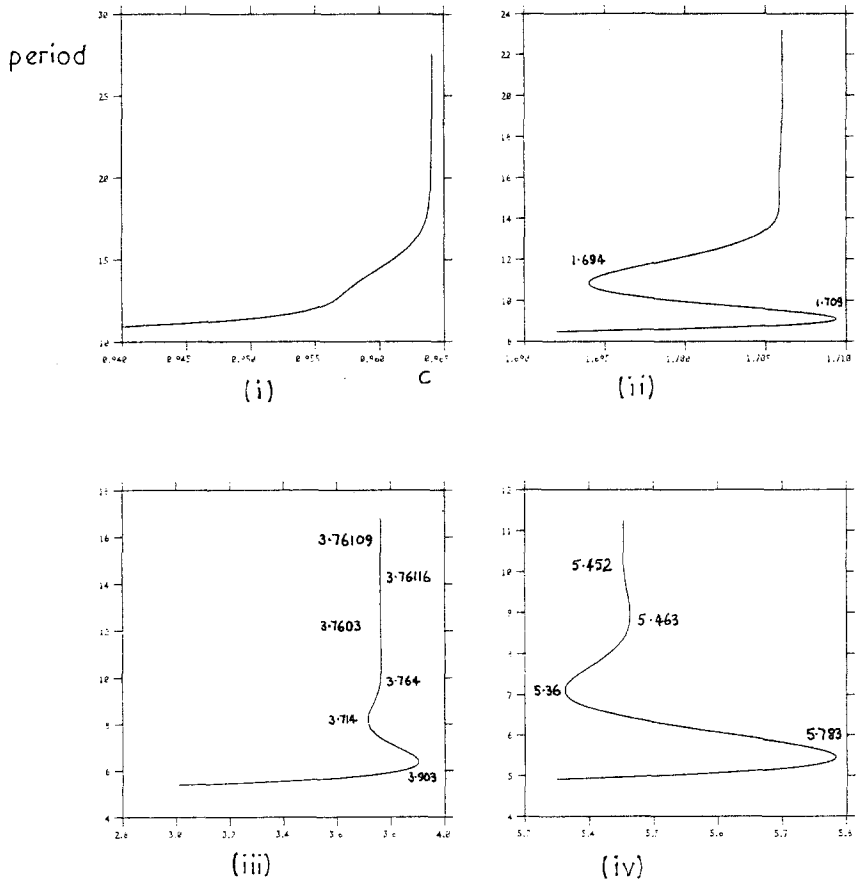

Fig. 4.7. Period of the principal period orbit plotted against c as the orbit approaches homoclinicity. (i) $b = 0.5$; (ii) $b = 0.8$; (iii) $b = 1.5$; (iv) $b = 2.0$. The numbers give c values at which saddle node bifurcations occur.

Although the upper portions of all the curves in Fig. 4.7 look similar, Figs. 4.7(i) and 4.7(ii) actually show the direct $\delta > 1$ approach to homoclinicity whereas Figs. 4.7(iii) and 4.7(iv) ($\delta < 1$) continue to oscillate as indicated by the parameter values on the figures.

Observe that for $b = 0.5$ and $b = 2.0$ ($\delta = 1.29$ and $\delta = 0.94$, respectively) we have obtained figures similar to those which relate to the asymptotic local analysis (Fig. 3.2), whilst $b = 0.8$ ($\delta = 1.14$) gives results more like those of Section 3.3.2, which discussed the behavior further from homoclinicity and, in particular, for δ near to one.

4.2.3. Stability. The linearized eigenvalue equation at the origin for the system (18) is

$$\lambda^3 + \lambda^2 + b\lambda - c = 0 \tag{20}$$

Thus it is impossible to have $\delta < 1/2$ (since if λ_1 is the real eigenvalue and $-\lambda_2$ is the real part of the complex conjugate eigenvalues, $\lambda_1 - 2\lambda_2 = -1$), so we are only interested in the stability predictions of Section 3.1.3 in $\delta > 1$ and $1 > \delta > 1/2$.

(i) $\delta > 1$ ($b = 0.5, 0.8$). The analysis of Section 3.1.3 predicts that the orbit will be stable as it approaches homoclinicity with increasing c. Therefore, if the orbit loses stability after the Hopf bifurcation (which it does, by period doubling, for all four b values we investigated) it must be restabilized before its final approach to homoclinicity. For both $b = 0.5$ and $b = 0.8$ this restabilization is achieved by a reverse period-doubling bifurcation. Numerical experiments confirm that the principal periodic orbit remains stable once it starts its final asymptotic approach to the homoclinic orbit.

(ii) $1 > \delta > 1/2$ ($b = 1.5, 2.0$). Figure 4.8 shows the stability of the principal periodic orbit as it approaches homoclinicity for $b = 1.5$. The diagram was constructed by calculating the Floquet exponents of the principal periodic orbit numerically whilst following it as it approaches homoclinicity.

As we follow the principal periodic orbit from one saddle-node bifurcation to the next along the branches of the curve which go from left to right with increasing period, the orbit is initially stable, then loses stability in a period-doubling bifurcation and is eventually restabilized in a reverse period-doubling bifurcation before reaching the next saddle node bifurcation. Along the other branches (right to left with increasing period) the orbit is always nonstable. All this is as predicted in the local analysis of Section 3.1.3. Compare Fig. 4.8 with Fig. 3.4 remembering that $\mu > 0$ corresponds to $c < c_b$.

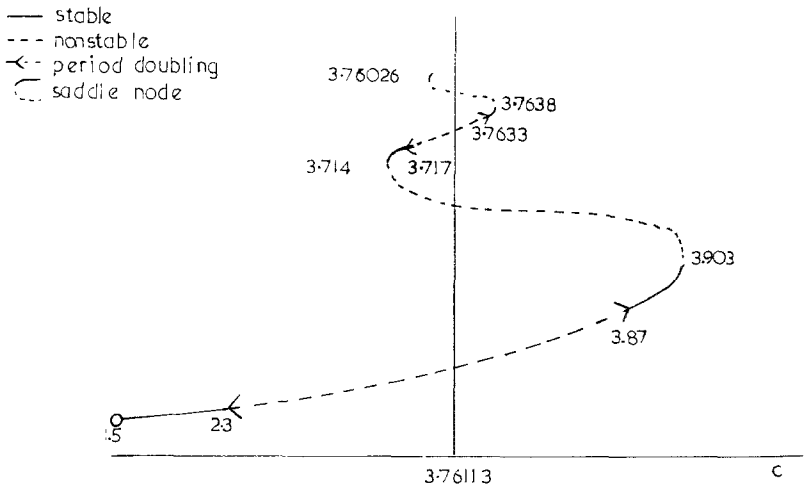

Fig. 4.8. The stability of the principal periodic orbit as it approaches homoclinicity with $\delta < 1$, $b = 1.5$.

4.2.4. Subsidiary Homoclinic Orbits. Near a homoclinic orbit with $\delta < 1$, Section 3.2 predicts sequences of subsidiary homoclinic orbits with increasing numbers of twists about the origin as c approaches c_b from below. For $b = 1.5$ and $b = 2.0$ we have located some of the double-pulse subsidiary homoclinic orbits; those we have observed spiral only a very small number of times about the stationary point, and consequently are the outermost ones (those with largest μ) predicted by the local analysis. The geometric ratio, $\exp(-\pi\lambda_1/\omega)$, which controls the rate of convergence of parameter values for which double-pulse homoclinic orbits occur is small (≈ 0.1), so it is not surprising that very few such orbits can be observed. In fact, the whole sequence of observed homoclinicities, from outermost double-pulse subsidiary to principal, occurs in a very small parameter range ($3.76105 < c < 3.76113$ when $b = 1.5$). We do observe other homoclinic orbits at parameter values further from homoclinicity (in $c < c_b$), but we shall not discuss these as subsidiary homoclinic orbits for reasons explained below.

4.2.5. The Global Bifurcation Picture. We need to go beyond the local analysis if we are to understand the global bifurcation picture and the occurrence of numerically observable chaos. At present no general method exists so we proceed by prudent numerical experiments.

Observe that the upper branches of the bifurcation curves in Fig. 4.7 occupy a very small range of parameter values close to the principal

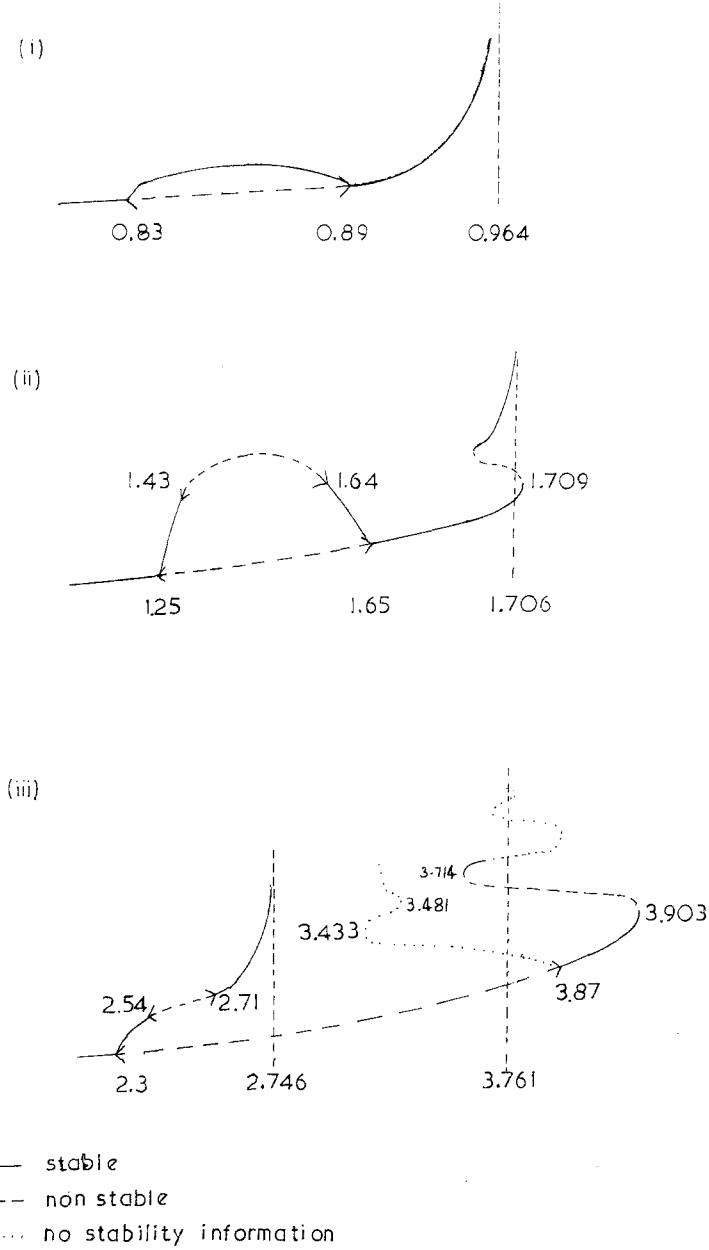

Fig. 4.9. Schematic bifurcation curves (at fixed b) for the principal periodic orbit and orbits which bifurcate from its lowest branch. Parameter values on the figure are the relevant c values. (i) $b = 0.5$; (ii) $b = 0.8$; (iii) $b = 1.5$.

homoclinic value. These ranges do not include values where chaos is observed numerically. Consequently, we concentrate on the lowest branch of the bifurcation curves shown in Fig. 4.7 and the orbits which bifurcate from it (bifurcations on this branch of the curve do occur on either side of interesting behavior). It is worth noting that with this emphasis it is not particularly important whether we have $\delta < 1$ or $\delta > 1$ at principal homoclinicity; despite the change in the local asymptotic analysis with changing δ, the behavior on the lowest branch will change smoothly as the parameters vary and, in some sense, we may consider the development independently of the other changes occurring in the system. The lowest branch, being further from principal homoclinicity, is also the branch on which one is most likely to find deviations from the predictions of Section 3, and this is another reason for studying it (cf. Section 3.3.2). A schematic view of the bifurcation diagrams for $b = 0.4$, 0.8, and 1.5 is given in Fig. 4.9.

When $b = 0.5^{(3)}$ the principal periodic orbit loses stability in a period-doubling bifurcation. The stable doubly periodic orbit produced in this bifurcation looks like the one shown in Fig. 4.10(i). This orbit remains stable until it restabilizes the principal periodic orbit in a reverse period-doubling bifurcation, and then the principal periodic orbit approaches homoclinicity as was shown in Fig. 4.7(i).

The path with $b = 0.8^{(3)}$ starts out like $b = 0.5$, but the orbit born in the period-doubling bifurcation loses stability in a further period-doubling bifurcation [Fig. 4.9(ii)]. There is then a sequence of period-doubling bifurcations leading to numerically observable chaos, despite the fact that $\delta > 1$ at homoclinicity. Chaotic trajectories look similar to that displayed in Fig. 4.10(ii) which has $b = 2.0$. This sequence of bifurcations then reverses,

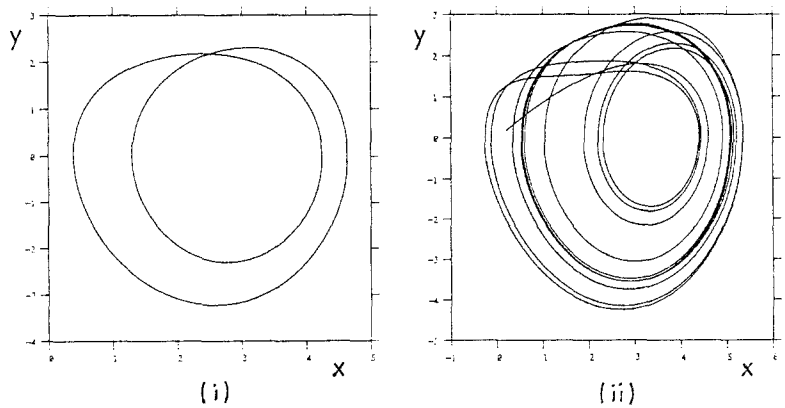

Fig. 4.10. (i) A double periodic orbit; $b = 2.0$, $c = 3.26$. (ii) A chaotic trajectory; $b = 2.0$, $c = 3.69$.

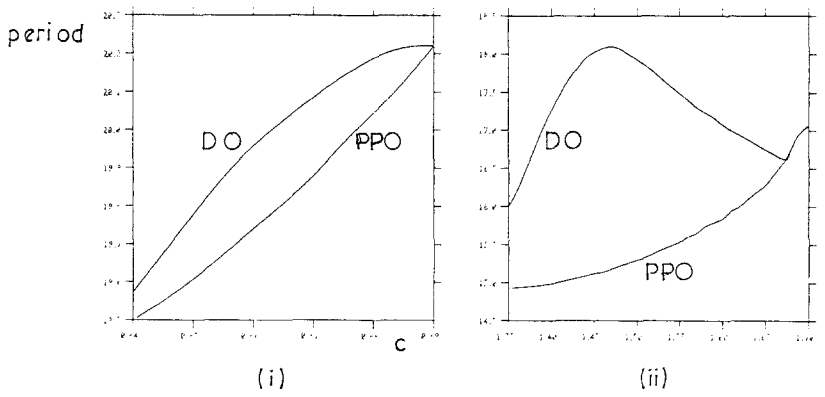

Fig. 4.11. The period of the doubled orbit (DO) was plotted with two times the period of the principal periodic orbit (PPO) for $b = 0.5$ and $b = 0.8$. Note the development of a bump. (i) $b = 0.5$; (ii) $b = 0.8$.

eventually restabilizing the principal periodic orbit. In particular, we have followed the orbit created by the first period-doubling bifurcation through the chaotic regime and it is, indeed, the orbit which restabilizes the principal periodic orbit. In Fig. 4.11 we have plotted the period of this doubled orbit, together with two times the period of the principal periodic orbit, against the parameter c. Notice the difference in shape of the two graphs. When $b = 0.8$ the period of the doubled orbit no longer stays close to twice the period of the principal periodic orbit, but has developed a bump. We shall see shortly that this heralds an important change in the bifurcation sequence. Once the principal periodic orbit has restabilized it approaches the principal homoclinic orbit as was shown in Fig. 4.7(ii).

At $b = 1.5$ [Fig. 4.9(iii)] we observe the sequence of period-doubling, chaos and reverse period-doubling bifurcations as before, eventually restabilizing the principal periodic orbit on the lowest branch of the wiggly curve shown in Fig. 4.7(iii). However, the periodic orbit created by the first period-doubling bifurcation is not the orbit which restabilizes the principal periodic orbit. If we follow the former we find it approaches a homoclinic orbit with an extra loop about the second stationary point, B. See Fig. 4.12(i), which shows this orbit close to homoclinicity. Similarly, the orbit which restabilizes the principal periodic orbit can be followed back to a (different) homoclinic orbit with an extra loop [Fig. 4.12(ii)]. This sequence of bifurcations appears essentially unchanged when $b = 2.0$.

The extra loop of these homoclinic orbits does not pass close to the origin and they occur at parameter values far from principal homoclinicity, so we believe that the existence of such orbits cannot properly be deduced

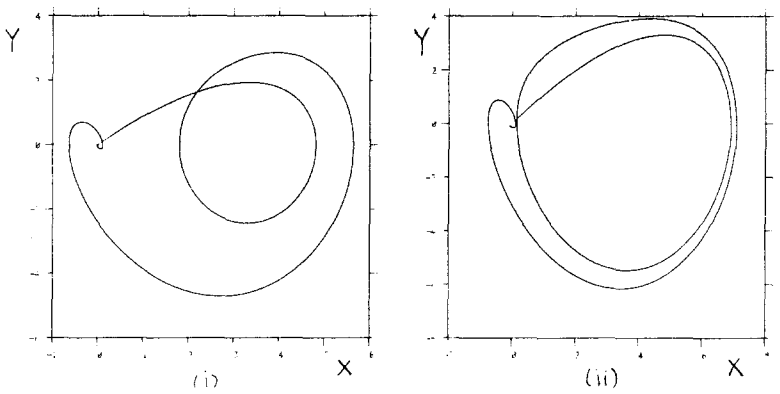

Fig. 4.12. The simplest secondary homoclinic orbits. (i) $b = 2.0$, $c = 3.8332$. (ii) $b = 2.0$, $c = 5.083$.

from the local analysis of the principal homoclinic orbit. In particular, it is probably not reasonable to think of them as subsidiary homoclinic orbits; we shall call homoclinic orbits such as those in Fig. 4.12 *secondary homoclinic orbits*. These orbits bifurcate from the lowest branch of the principal periodic orbit so they will also play an important role in the observable dynamics of the system.

We believe that for b values between 0.8 and 1.5, the bump on Fig. 4.11(ii) gets bigger until at some critical b value it becomes infinite. At larger b values we get a pair of secondary homoclinic orbits and thereafter the bifurcation sequence looks like Fig. 4.9(iii). For $b = 1.5$ both secondary homoclinic orbits are in the region of parameter space with $\delta > 1$. For larger b values one or both of these homoclinic orbits may have $\delta < 1$ with the consequent complications. Our claim (Section 3.3.2) that each homoclinic orbit only contributes one periodic orbit to the global bifurcation picture makes this relatively unimportant as far as that picture is concerned.

We believe that there is an infinite sequence of secondary homoclinic orbits in a region of parameter space as shown in Fig. 4.13, with the simplest secondary homoclinic orbits (Fig. 4.12) on the inside. This suggestion will be supported by the arguments of Section 4.3. Each of these secondary homoclinic orbits has different global properties, so this is not the same phenomenon as the occurrence of subsidiary homoclinic orbits discussed in Section 3.2; each secondary homoclinic orbit will, of course, have its own subsidiary orbits if it occurs in the region $\delta < 1$. We have not established the arrangement of all the secondary homoclinic orbits within the region A of Fig. 4.13; the figure shows some of the possibilities likely to occur.

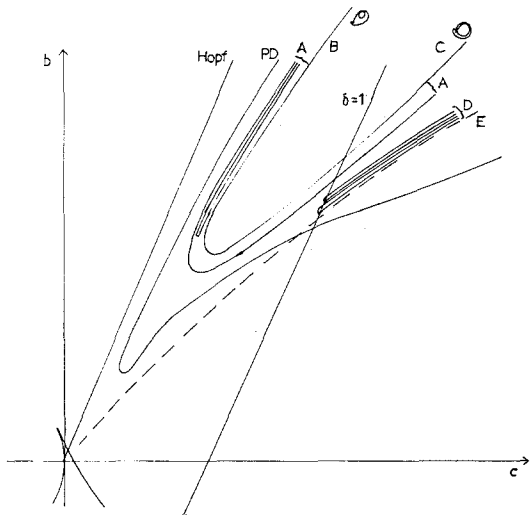

Fig. 4.13. The global bifurcation diagram. PD, the first period-doubling bifurcation; A, secondary homoclinic orbits; B, locus of the secondary homoclinic orbit shown in Fig. 4.12(i); C, locus of the secondary homoclinic orbit shown in Fig. 4.12(ii); D, subsidiary homoclinic orbits; E, principal homoclinic orbit.

As we increase c at a fixed b value large enough to intersect the innermost curve of secondary homoclinic orbits, we first observe a sequence of period-doubling bifurcations leading to the familiar chaotic regime. This contains intervals of parameter values where stable periodic orbits are observed, and others where chaotic behavior is observed (cf. most chaotic systems). We then reach the left-hand (small c) edge of the region of secondary homoclinic orbits. From this point onwards we expect some trajectories to escape to infinity (having arrived at the wrong side of the stable manifold of the origin). The effect of this sequence of homoclinic orbits is to remove periodic orbits from the system, eventually leaving [once we have crossed the innermost curve which corresponds to the homoclinic orbit of Fig. 4.12(i)] only the nonstable principal periodic orbit (cf. Section 4.3). Numerical observations do not detect a sudden change in the behavior of the system when we reach the beginning of this sequence; trajectories may wander chaotically for a very long time before escaping to infinity or (particularly if $\delta > 1$ in this region) they may be attracted to various periodic orbits which are stable because they are approaching homoclinicity; some of these orbits may be extremely complicated and chaotic looking.

The sequence of secondary homoclinic orbits on the right (larger c) then produces the orbits which restabilize the principal periodic orbits on the lowest branch. There may be stable chaotic behavior in this region also

(to the right of the secondary homoclinic orbits), but we have not observed it and we do expect many trajectories to escape to infinity.

Arneodo *et al.*[3] were aware of the existence of some secondary orbits and suggested that these came from the doubly periodic orbits as described above. However, Fig. 4.13 shows the global bifurcation picture in a much more complete form than the one given by Arneodo *et al.*[3]

Near parameter values for which the principal homoclinic orbit exists with $\delta < 1$, we know from the local analysis that there must exist many periodic orbits. We have, however, been unable to observe stable chaotic motion near the principal homoclinic orbit; many of the periodic orbits are nonstable and most trajectories eventually leave the region of phase space near the origin. Any stable chaotic behavior that exists must have a very small basin of attraction, and must be stable over very small parameter ranges.

We believe that for large enough c (to the right of a neighborhood of the principal homoclinic orbit) *no* periodic orbits exist and all trajectories escape to infinity.

4.2.6. Further Remarks. We have drawn a distinction between the secondary homoclinic orbits and the subsidiary homoclinic orbits on the grounds that the secondary homoclinic orbits' extra loops about B do not pass close enough to the origin to be treated by local analysis. As we shall discuss in the concluding section, the results in this section and Section 4.3 are essentially compatible with the results we would have obtained by treating the secondary homoclinic orbits as "extremely distant" subsidiary homoclinic orbits of the principal homoclinic orbit. We continue, however, to think this separation reasonable for reasons discussed above and expanded upon in Section 5.

4.3. A Piecewise Linear System of Rössler

It is our intention, in this section, to study a one-parameter piecewise linear system of ordinary differential equations which has a global bifurcation picture which is almost exactly the same as that of the example studied in Section 4.2 with c varying and b large enough (e.g., $b = 2.0$). Rössler *et al.*[18] introduced the system, and it was later studied and described in Sparrow,[19] Rössler,[20] and Uehleke.[21] The system is very similar to piecewise linear systems studied independently by Arneodo *et al.*[22] and the techniques used in the last-mentioned paper to prove the existence of homoclinic orbits of the type discussed in this paper are also applicable to the earlier papers. As Arneodo *et al.*[22] point out, the development of chaos in these systems is somewhat similar to the development of chaos in

many of the simpler known chaotic systems (e.g., Ref. 23), suggesting, as with the example from Section 4.2, that the role of homoclinicity in the development of numerically observed chaos deserves further study. Sparrow[19] did recognize that homoclinicity had a role to play in the understanding of the system to be described below. However, in that paper the development of chaos was studied by considering a global one-dimensional approximate return map derived from an analysis of the behavior which centered on the other (i.e., the nonhomoclinic) stationary point in the system. It is this analysis which we now wish to describe. When homoclinicity enters the picture we shall treat it in a global and not a local way. In other words, we shall assume that each homoclinic bifurcation produces or destroys just one periodic orbit from our global picture and that we are not overly concerned with the local details. We only describe the system and derivation of the map briefly below, since full details can be found in Ref. 19. We will then discuss the interrelationship between the approach of this section (4.3) and the approach of the previous section (4.2).

4.3.1. The System. The system we study is

$$\dot{x} = f(z) - x$$
$$\dot{y} = x - y$$
$$\dot{z} = y - z$$

where $f(z)$ has the form

$$f(z) = a - b(z - p), \qquad z \leqslant p$$
$$= a + c(z - p), \qquad z \geqslant p$$

Sparrow[19] used parameter values $a = -0.25$, $p = 3/7$, $b = 8.4$, and $c = 8.4r$ with $2 < r < \infty$, since these were the values used by Rössler *et al.*[18] In what follows the exact values are probably not important except that we take $a < p$, $b > 8$, and $c > 1$ so that there are two nonstable stationary points, one in the linear system which lies above the plane $z = p$ and one in the linear system which lies below $z = p$.

We call the two stationary points O and B (in direct analogy with the example of Section 4.2); O lies in $z > p$ and B lies in $z < p$. The eigenvalues at O are $c^{1/3} - 1$ (which is real and positive) and the complex conjugate pair, $-1 - \frac{1}{2}c^{1/3} \pm i\omega_0$, which have negative real part.

Thus, if O has a homoclinic orbit it is amenable to the analysis of this paper. We concentrate, however, on the other stationary point, B, which has one real and negative eigenvalue $(-b^{1/3} - 1)$ and a complex conjugate pair of eigenvalues, $\frac{1}{2}(b^{1/3} - 2) \pm i\omega_1$, which have positive real part if $b > 8$. Figure 4.14 shows the stable and unstable manifolds of these

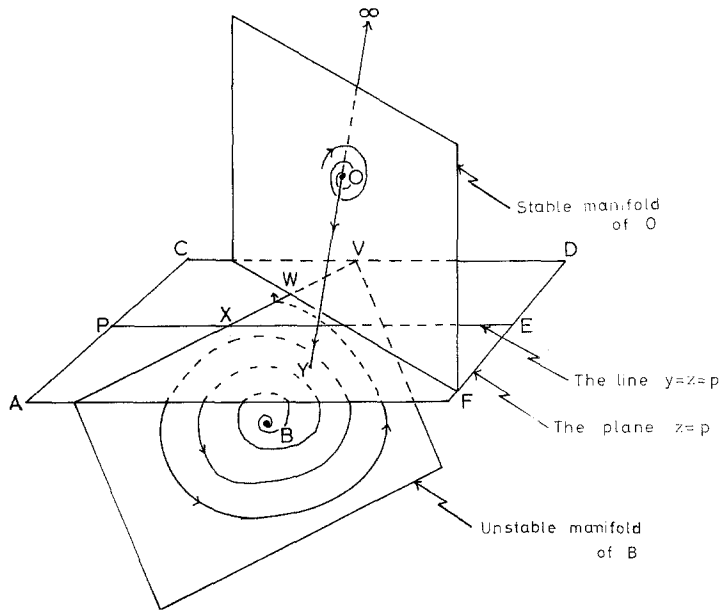

Fig. 4.14. A schematic picture of the piecewise-linear system. The system is linear above and below the plane $z = p$ (which includes $ACDF$) and parts of the stable and unstable manifolds of the stationary points 0 in $z > p$ and B in $z < p$ are shown.

stationary points in the half-spaces $z < p$ and $z > p$ in the case where $b > 8$. We will be interested in trajectories which behave as follows:

(i) A trajectory started on $z = p$ in APEF will travel downwards ($y < p$ and $\dot{z} = y - z < 0$). Below the plane $z = p$ it will move rapidly towards the unstable manifold of B and spiral slowly outwards, eventually striking the plane $z = p$ again somewhere near the line XV.

(ii) It will then move in the half-space $z > p$ under the influence of the point O. If it has struck $z = p$ near the section XW of XV, it will inevitably return to $z = p$ again, somewhere close to an arc from X to Y (Y is the point where one branch of O's unstable manifold first strikes $z = p$) since the effect of the linear system in $z > p$ will be to map points on XW onto an arc from X to Y. The trajectory is now on $z = p$ in APEF again and we can go back to (i) with the possibility of the trajectory remaining bounded forever. If, however, the trajectory comes up through $z = p$ near to the section VW of XV, that trajectory will probably be lost, tending to infinity close to the other branch of the unstable manifold of O.

4.3.2. A One-Dimensional Map. We can extract a one-

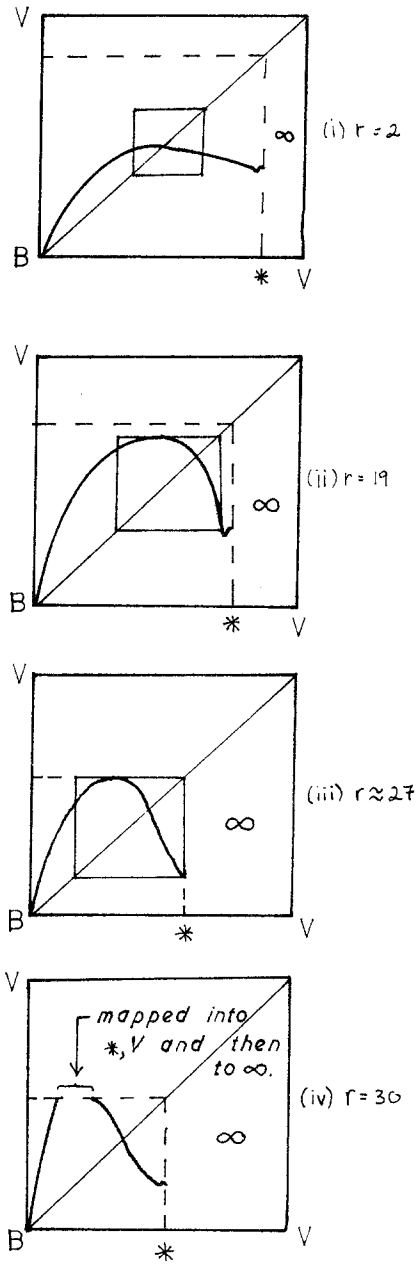

Fig. 4.15. Approximate one-dimensional return maps of the line BV to itself for the piecewise linear system $b = 8.4$, $a = -0.25$, $c = 8.4r$. The map is not defined in $(*, V)$. (i) $r = 2$; (ii) $r = 19$; (iii) $r \approx 27$; (iv) $r = 30$.

dimensional map which models the behavior of this system if we assume that trajectories below $z = p$ are attracted instantaneously to the unstable manifold of B. This is a reasonable approximation when the parameter $b = 8.4$ since we then have very slow outwards spiraling on the unstable manifold of B [the real part of the complex eigenvalues is $\frac{1}{2}(b^{1/3} - 2)$] and relatively rapid movement towards this manifold (the real eigenvalue at B is $-b^{1/3} - 1$). We then compute a first return map on a line such as BV. BV lies on the unstable manifold of B and trajectories started on BV will strike the plane $z = p$ along the line XV; those trajectories striking $z = p$ along WV will be lost so the map is not defined everywhere. The simplicity of our system means we can compute these maps with arbitrary accuracy, and maps calculated with the parameter values given above ($a = -0.25$, $b = 8.4$, $c = 8.4r$) give results which model the actual behavior of the system very well.[19] This modeling was not only qualitative but quantitative; the development of chaos in the one-dimensional maps gave good predictions for the parameter values at which chaos developed in the complete system.

Maps similar to those calculated in Ref. 19 are shown in Fig. 4.15. The parameter r referred to in Fig. 4.15 is the one above ($c = 8.4r$) and the parameters a and b are fixed.

The point (*) marked on each of the diagrams of Fig. 4.15 is the point on BV such that the trajectory started at (*) strikes the plane $z = p$ exactly at W (which moves as r moves). On striking $z = p$ at W a trajectory will spiral into the stationary point O and not return to BV; therefore the map is not defined at (*). The map is also undefined for points between (*) and V; trajectories started at these points strike $z = p$ along WV and are lost to infinity. The map is defined, however, for points between B and (*); trajectories started at these points strike $z = p$ along XW and return to BV as described above. Observant readers will notice that the map has a small hiccup for points close to and on the left of (*). In fact, we know there must be an infinite number of very small oscillations as we approach (*); these correspond to the large amount of spiralling which trajectories can do in the half-space $z > p$ if they arrive at $z = p$ close enough to W.

In Figs. 4.15(i) and 4.15(ii) we have drawn an inner box; points within these boxes map onto other points within the boxes, which therefore give us a region in which we can expect to find bounded trajectories. The point (*) lies outside the boxes and does not interest us yet. At $r = 2$ [Fig. 4.15(i)] we have a stable fixed point (representing a stable periodic orbit of the system) and there are then successive period-doubling bifurcations as r increases leading to a chaotic one-dimensional map and a chaotic system at $r = 19$ [Fig. 4.15(ii)]. We claim that this development is similar to the development of the example in Section 4.2 as the parameter c there increased from the

Hopf bifurcation value towards the leftmost homoclinic curve of Fig. 4.13 (at some large enough b value).

Reaching the leftmost homoclinic curves of Fig. 4.13 corresponds to reaching diagram (iii) of Fig. 4.15. Now, for the first time, the point (*) becomes of interest. The unstable manifold of the stationary point O will, in our one-dimensional approximation of the system, first strike BV at $g(*)$. [Here we are writing $g(\cdot)$ for the maps of Fig. 4.15.] Since our map is chaotic we expect that as we follow successive iterates of this point $g^2(*)$, $g^3(*)$, etc., we will at some point end up with $g^n(*) \approx (*)$. For an appropriate choice of parameters we will have $g^n(*) = (*)$ for some n, and this condition will be equivalent to the condition for the stationary point O to have a homoclinic orbit. As we move on to Fig. 4.15(iv) we have more and more of these homoclinic parameter values, and it is clear that as we pass through each such value we lose a periodic orbit from our global picture. Finally we reach the position shown in Fig. 4.16(i) where we have a homoclinic orbit of "period two" [this corresponds to the homoclinic orbit of Fig. 4.12(i)] and for slightly larger parameter values we have the situation shown in Fig. 4.16(ii) in which it is clear that there can be no periodic orbits in our map except for the fixed point (which represents the principal periodic orbit of Section 4.2). In the whole parameter range represented by Figs. 4.16(i) to 4.16(ii) we expect most trajectories to be unbounded; we have lost the turning point of our map (which is the part that gives stability to the periodic orbits) and the chaotic nature of the flow will ensure that most trajectories eventually fall into the "escape region."

The last paragraph does, of course, ignore some complicated considerations which we must now face. If we concentrate on the point (*) we must be prepared to consider the complicated nature of the map to the left of (*); that is, the infinite number of very small oscillations there. If we were to analyze exactly what occurred as we passed through homoclinic parameter values we would need to know the shape of these oscillations (which would depend on δ, the ratio of the real parts of the eigenvalues at O), and the analysis would turn into a one-dimensional version of the local analysis of each homoclinic orbit. In the case of our example we would have $\delta < 1$ for all the homoclinic orbits which occur (which does differ from the example of Section 4.2) and would expect to find an infinite series of saddle-node bifurcations on either side of the homoclinic values, together with other complications deducible from the local analysis and all due to the small oscillations near (*). We claim, however, that from the point of view of our global picture it makes perfectly good sense to ignore the small oscillations and note that as we move the parameter through some reasonably small interval about the homoclinic values the global effect is just the

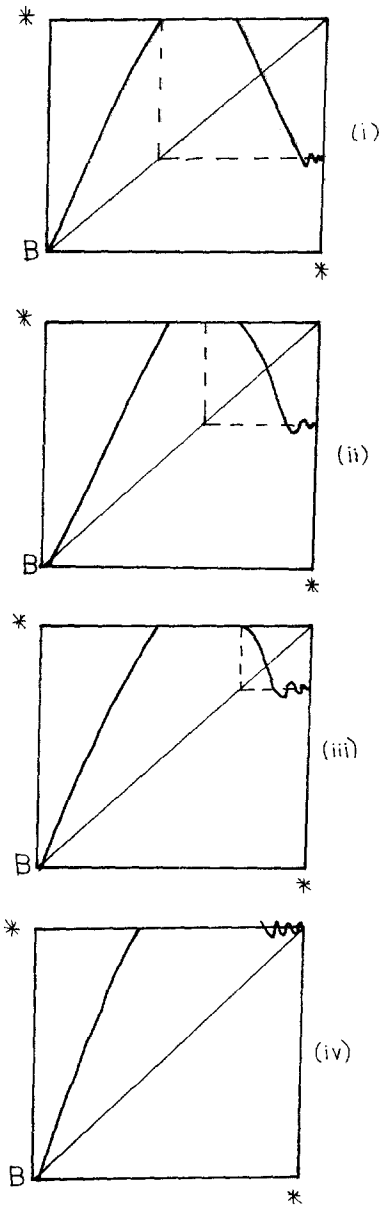

Fig. 4.16. The approximate one-dimensional map, as r increases beyond 30, for the interval $[B, *]$. (i) There is a homoclinic orbit of "period 2" [cf. Fig. 4.12(i)]. (ii) The fixed point is the only periodic point in the system. (iii) There is another homoclinic orbit of "period 2" [cf. Fig. 4.12(ii)]. (iv) Principal homoclinicity is reached.

removal of the one periodic orbit. In this case, of course, the value of δ and the shape of the oscillations is irrelevant. Before discussing this a little further let us see what happens if we continue to develop the global map beyond the situation shown in Fig. 4.16(ii).

In Fig. 4.16(ii) we have reached the situation where we may have homoclinic orbits occurring on only the right-hand piece of our disconnected one-dimensional map. The first to occur will be another "period two" homoclinic orbit as shown in Fig. 4.16(iii), and this corresponds to Fig. 4.12(ii) of Section 4.2. At this point homoclinic orbits have started adding periodic orbits to our global picture, and if we continue in this direction this corresponds to crossing over the right-hand side of the looped homoclinic curves of Fig. 4.13 until we eventually arrive at Fig. 4.16(iv). Figure 4.16(iv) is, of course, the map we would want to consider if we were to do a one-dimensional local analysis of the last homoclinicity to occur (the principal homoclinicity) and sufficiently beyond the parameter value for Fig. 4.16(iv) we expect there to be no bounded trajectories at all; the last homoclinicity has swallowed up the orbit which was represented by the fixed point of the one-dimensional map (the principal periodic orbit, just as in Section 4.2) and all trajectories escape to infinity.

4.3.3. Further Remarks. We have chosen a piecewise linear example for this section because of the ease of analysis. We do expect, however, that it would have been almost as easy to extract (numerically) a one-dimensional approximation for the example of Section 4.2, and that the map so obtained would have behaved in basically the same way as that studied here. The correspondence between the global results of the two sections certainly encourages this expectation. We have, therefore, a different method of looking at the example of Section 4.2, and must examine the implications of this approach.

It would be possible to claim that the big, global-chaos-generating hump in our one-dimensional map is just another of the infinite number of oscillations that spread out from (*), the "homoclinic point." This would basically be equivalent to the claim that the local analysis of the principal homoclinicity predicts numerically observable chaos at parameter values far from homoclinicity. In line with our remarks throughout this paper, we do not really support such a claim. Notice, in particular, how the behavior of the flow near the stationary point B (which gets no mention in the homoclinic analysis) was crucial to our being able to extract a global approximate one-dimensional map in the first place. In addition, we managed to explain the appearance of chaos (with increasing parameter) almost entirely without reference to the stationary point O. We could, if we

liked, refer to our approach in this section (4.3) as a B-centered approach, while the approach in Section 4.2 was O-centered. For further discussion the reader is referred to the next, and final, section.

5. CONCLUSION AND OTHER SYSTEMS

In this paper we have derived some new results from the local analysis of the behavior near a homoclinic orbit to a stationary point of saddle-focus type and shown how these results, particularly insofar as they relate to the simpler periodic orbits in the system and in conjunction with numerical methods for following these periodic orbits with changing parameter, can be used to piece together global bifurcation pictures. We hope this approach will be useful in the study of many systems.

From the examples we have considered, and from other literature (see below), it is clear that we must expect the observable effects of the existence of a homoclinic orbit in a system to vary quite a lot, though certain general patterns can be expected fairly frequently. In the examples of Sections 4.2 and 4.3 we found that virtually all the interesting observable behavior (in particular, stable chaotic motions) was associated with the lowest branch of the bifurcation curve of the principal periodic orbit, and occurred at parameter values far from principal homoclinicity. Perhaps remarkably, then, it seems that all our results for the system of Section 4.2 *are* compatible with predictions from a local analysis of the principal periodic orbit. The homoclinic orbits we called secondary (attempting to separate local and global pictures) could equally well have been considered subsidiary (apart from the fact that we could not convince ourselves that the orbits in Fig. 4.12 passed close to the origin twice) *with the same result*. Nonetheless, the fact that we could analyze a very similar system in a completely different way in Section 4.3, suggests that these features are the result of a global interaction between the stationary points, and are not just a necessary consequence of homoclinicity in the system.

Interestingly, global bifurcation pictures similar to that shown in Fig. 4.13 have been discovered in other systems. Knobloch and Weiss[24] computed a bifurcation diagram for a five-dimensional model of magneto-convection which looks remarkably like that of Fig. 4.13 and which contains homoclinic and heteroclinic orbits (the system has a symmetry). A. Bernoff[25] has followed several periodic orbits in a related four-dimensional system and confirms that they behave in a similar way to the analogous orbits in our examples. In their paper, Knobloch and Weiss[24] refer to "gaps," "bubbles," and the propensity of bubbles to "burst." *Bifurcation bubbles* are the sequences of bifurcations occurring for low b

values in the example of Section 4.2; in other words, when a stable periodic orbit period-doubles (with possibly a finite number of further period-doublings) and then that sequence of bifurcations reverses itself eventually restabilizing the original orbit, that whole sequence of bifurcations is a bubble. If there is an infinite sequence of period-doublings leading to chaos within the bubble, then Knobloch and Weiss say the bubble has *burst*. As b is increased (Section 4.2), secondary homoclinic orbits start to occur in the sequence of bifurcations and a parameter range appears in the middle of the bubble where no stable behavior (chaotic or otherwise) is observed; this parameter range is a *gap*, and corresponds to the section within the locus of secondary homoclinic orbits in Fig. 4.13 where we claim that the nonstable principal periodic window is the only periodic orbit in the system. See also Ref. 26.

Of perhaps even greater interest is the bifurcation diagram in Ref. 27, computed for a partial differential equation modeling two-dimensional thermosolutal convection, which appears to show, quite clearly, bifurcations on the two lowest branches of a bifurcation curve for some principal periodic orbit approaching a $\delta < 1$ homoclinicity. Regrettably, it is not yet possible to follow periodic orbits in the solution to partial differential equations in the same way as is possible for o.d.e.'s, so these remarks remain speculative. Note, however that this bifurcation picture is different from any that we have observed numerically, adding weight to our claim that homoclinicities will have different effects on different systems.

Returning to three-dimensional systems with two stationary points, variations are possible here also. Gaspard and Nicolis[28] and Gaspard, Kapral, and Nicolis[29] have looked at one of Rössler's systems[23] with a view to determining the effect of homoclinicities in that system. The parameter range they examine does not seem to include values at which principal homoclinicity (in the sense of this paper) occurs, though the bifurcations they observe are compatible with the left side of a figure like Fig. 4.13 up to the point where secondary homoclinic orbits start to occur and attracting behavior is no longer observed. Our analysis suggests that the selection of one particular secondary homoclinic orbit as causing the loss of attractivity is probably difficult. It should be noted that the occurrence of infinitely many secondary homoclinic orbits in a small parameter range is a quite different phenomenon from the occurrence of infinitely many subsidiary homoclinic orbits which would be associated with each of the secondary homoclinic orbits if $\delta < 1$; the former is a global phenomenon, the latter a local one. Gaspard and Nicolis[28] also observe homoclinic trajectories to the other stationary point (B in our examples) which appear to be associated with the change-over from Rössler's "spiral-

type" to "screw-type" chaos (Ref. 23; see also Ref. 22). In a very recent paper[29] they investigate the bifurcations near such homoclinicities in some detail. Notice, though, that it is fairly easy to see that if a piecewise linear system like that studied in Section 4.3 were adjusted so that there were homoclinic orbits to the point B (see Fig. 4.14) as well as to O, then the existence of homoclinic orbits to B would tend to change the nature of the chaotic attractor (by ensuring that trajectories continually passed very close to B) rather than creating or destroying attractivity. It should be noted that these remarks have a global rather than local character and the δ values at the homoclinic orbits to B would seem likely to be relatively unimportant. Further information on the possibilities of piecewise linear systems, though with a slightly different emphasis from ours here, can be found in Ref. 21.

Our other example, the Lorenz equations (Section 4.1), illustrated the fact that the homoclinicities may occur in systems where they are relatively unimportant for the understanding of the majority of the observed behavior. In such cases it may make sense, as we have suggested, to think of the principal homoclinicity (and any complications associated with it) as producing a single periodic orbit.

In conclusion, then, homoclinic orbits may be considered in both local and global terms. Often the local considerations, such as $\delta < 1$ or $\delta > 1$, and the results of Sil'nikov consequent upon them, do not tell us much about the behavior likely to be observed in the system; we have argued that this is particularly likely to be the case if the quantity $\pi\lambda_2/\omega$, calculated from the eigenvalues at the relevant stationary point, is large. Global considerations are likely to be much more important; thus, for instance, we can speak of observable chaos occurring close to sequences of secondary homoclinic orbits (which each have, globally, quite different properties), without particular reference to whether $\delta < 1$ or $\delta > 1$ for each of these orbits (cf. Sections 4.2 and 4.3). It is possible that certain global bifurcation pictures, in particular that shown in Fig. 4.13, will occur frequently in systems with homoclinicities, but we can expect global variations on this figure (such as must occur with Rössler's sytem) which cannot be predicted by the local analysis of any one homoclinic orbit; consequently, we refer to Fig. 4.13 as a global picture, despite the fact that in its essentials it appears to be compatible with local predictions from the analysis of the principal homoclinic orbit.

Further studies may illuminate other more general global bifurcation structures; for the moment, and particularly in more complicated or higher-dimensional systems, the existence of a homoclinic orbit of the type described here should not be taken to lead immediately to any global conclusions, but should be carefully investigated, probably by following periodic orbits of the system.

ACKNOWLEDGMENTS

We would like to thank Andy Bernoff, Edgar Knobloch, and Nigel Weiss for many useful discussions, and for explaining their numerical results to us. We would also like to thank Pierre Coullet, John Guckenheimer, Rober MacKay, and Ed Speigel, as well as those just mentioned, for reading through a first draft of this paper and making many helpful suggestions. Finally, we would like to thank Robert MacKay for first pointing out that we would improve the orbit-following technique we had been using. P.A.G. acknowledges the support of an SERC grant.

REFERENCES

1. L. P. Sil'nikov, A Case of the Existence of a Denumerable Set of Periodic Motions, *Sov. Math. Dokl.* **6**:163–166 (1965).
2. L. P. Sil'nikov, A Contribution to the Problem of the Structure of an Extended Neighborhood of a Rough Equilibrium State of Saddle-Focus Type, *Math. USSR Sbornik* **10**:91–102 (1970).
3. A. Arneodo, P. Coullet, E. Speigel, and C. Tresser, Asymptotic Chaos, Preprint, Universite de Nice (1982).
4. J. Guckenheimer, Multiple Bifurcation Problems of Codimension Two, Preprint, U.C. Santa Cruz (1980).
5. J. Guckenheimer, On a Co-Dimension Two Bifurcation, in *Dynamical Systems and Turbulence: Warwick 1980*, D. Rand and L.-S. Young, eds., Lecture Notes in Mathematics No. 898 (Springer-Verlag, Berlin, 1981).
6. P. Gaspard, Memoire de License, Universite de Bruxelles (1982).
7. A. Arneodo, P. Coullet, and C. Tresser, Possible New Strange Attractors with Spiral Structure, *Commun. Math. Phys.* **79**:573–579 (1981).
8. G. R. Belitskii, Equivalence and Normal Forms of Germs of Smooth Mappings, *Russ. Math. Surv.* **33**:107–177 (1978).
9. C. Tresser, thesis, Universite de Nice (1981).
10. H. W. Broer and G. Vegter, Subordinate Sil'nikov Bifurcations near Some Singularities of Vector Fields Having Low Codimension, Preprint ZW-8208, Rijksuniversitat, Groningen (1982).
11. J. A. Yorke and K. T. Alligood, Cascades of Period-Doubling Bifurcations: A Prerequisite for Horseshoes, Preprint, University of Maryland (1982).
12. P. Gaspard, Generation of a Countable Set of Homoclinic Flows Through Bifurcation, *Phys. Lett.* **97A**:1–4 (1983).
13. S. P. Hastings, Single and Multiple Pulse Waves for the Fitzhugh–Nagumo Equations, *SIAM J. Appl. Math.* **42(2)**:247–260 (1982).
14. J. Evans, N. Fenichel, and J. A. Feroe, Double Impulse Solutions in Nerve Axon Equations, *SIAM J. Appl. Math.* **42(2)**:219–234 (1983).
15. J. A. Feroe, Existence and Stability of Multiple Impulse Solutions of a Nerve Axon Equation, *SIAM J. Appl. Math.* **42(2)**:235–246 (1983).
16. C. Sparrow, *The Lorenz Equations: Bifurcations, Chaos and Strange Attractors*, Appl. Math. Sci. No. 41 (Springer-Verlag, New York, 1982).
17. E. N. Lorenz, Deterministic Non-Periodic Flows, *J. Atmos. Sci.* **20**:130–141 (1963).
18. R. Rössler, F. Gotz, and O. E. Rössler, Chaos in Endocrinology, *Biophys. J.* **25**:216A (1979).

19. C. Sparrow, Chaos in a Three-Dimensional Single Loop Feedback System with a Piecewise Linear Feedback Function, *J. Math. Anal. Appl.* **83**:275–291 (1981).
20. O. E. Rössler, The Gluing Together Principle and Chaos, in *Non-linear Problems of Analysis in Geometry and Mechanics*, M. Atteia, D. Bancel, and I. Gumowski, eds. (Pitman, New York, 1981), pp. 50–56.
21. B. Uehleke, Chaos in einem stuckweise linearen System: Analytische Resultate, Ph.D. thesis, Tübingen (1982).
22. A. Arneodo, P. Coullet, and C. Tresser, Oscillators with Chaotic Behavior: An Illustration of a Theorem by Sil'nikov, *J. Stat. Phys.* **27**:171–182 (1982).
23. O. E. Rössler, Continuous Chaos: Four Prototype Equations, in *Bifurcation Theory and Applications in Scientific Disciplines*, O. Gurel and O. E. Rössler, eds., Proc. N.Y. Acad. Sci. No. 316, pp. 376–394 (1978).
24. E. Knobloch and N. O. Weiss, Bifurcations in a Model of Magnetoconvection, *Physica* **9D**:379–407 (1983).
25. A. Bernoff, Preprint, University of Cambridge (1984).
26. E. Knobloch and N. O. Weiss, Bifurcations in a Model of Double-Diffusive Convection, *Phys. Lett.* **85A(3)**:127–130 (1981).
27. D. R. Moore, J. Toomre, E. Knobloch, and N. O. Weiss, Chaos in Thermosolutal Convection: Period Doubling for Partial Differential Equations, *Nature* **303**: (1983).
28. P. Gaspard and G. Nicolis, What Can We Learn from Homoclinic Orbits in Chaotic Dynamics? *J. Stat. Phys.* **31**:499–518 (1983).
29. P. Gaspard, R. Kapral, and G. Nicolis, Bifurcation Phenomena near Homoclinic Systems: A Two-Parameter Analysis, This Issue, *J. Stat. Phys.* **35**:697 (1984).